AD-A166 979 SUMMARY OF DIHEST (DIRECT INDUCED HIGH EXPLOSIVE SIMULATION TECHNIQUES) S.. (U) R AND D ASSOCIATES ARLINGTON VA J B WEBSTER 01 MAR 85 RDA-TR-135702-001 1/1

UNCLASSIFIED DNA-TR-85-239 DNA001-85-C-0025 F/G 18/3 NL

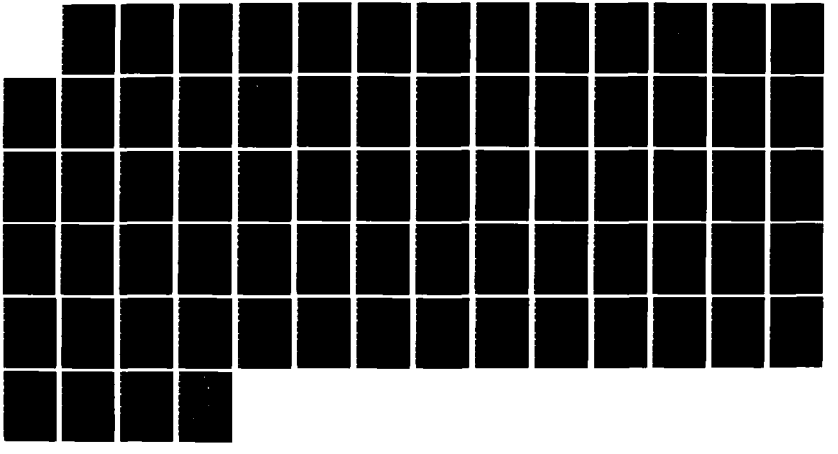

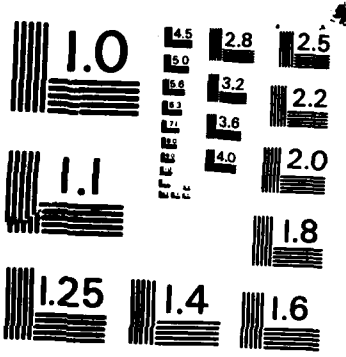

(12)

AD-A166 979

DNA-TR-85-239

SUMMARY OF DIHEST SIMULATOR EXPERIMENTS AND EFFORTS IN SUPPORT OF THE ADVANCED SILO HARDENING PROGRAM

J. Burton Webster, III
R & D Associates
1401 Wilson Blvd
Arlington, VA 22209-2381

1 March 1985

Technical Report

CONTRACT No. DNA 001-85-C-0025

Approved for public release;
distribution is unlimited.

THIS WORK WAS SPONSORED BY THE DEFENSE NUCLEAR AGENCY
UNDER RDT&E RMSS CODE B341085466 Y99QMXSC00041 H2590D.

Prepared for
Director
DEFENSE NUCLEAR AGENCY
Washington, DC 20305-1000

Destroy this report when it is no longer needed. Do not return to sender.

PLEASE NOTIFY THE DEFENSE NUCLEAR AGENCY, ATTN: STTI, WASHINGTON, DC 20305-1000, IF YOUR ADDRESS IS INCORRECT, IF YOU WISH IT DELETED FROM THE DISTRIBUTION LIST, OR IF THE ADDRESSEE IS NO LONGER EMPLOYED BY YOUR ORGANIZATION.

UNCLASSIFIED
SECURITY CLASSIFICATION OF THIS PAGE

A166 979

REPORT DOCUMENTATION PAGE

1a. REPORT SECURITY CLASSIFICATION UNCLASSIFIED	1b. RESTRICTIVE MARKINGS
2a. SECURITY CLASSIFICATION AUTHORITY N/A since Unclassified	3. DISTRIBUTION/AVAILABILITY OF REPORT Approved for public release; distribution is unlimited.
2b. DECLASSIFICATION/DOWNGRADING SCHEDULE N/A since Unclassified	
4. PERFORMING ORGANIZATION REPORT NUMBER(S) RDA-TR-135702-001	5. MONITORING ORGANIZATION REPORT NUMBER(S) DNA-TR-85-239
6a. NAME OF PERFORMING ORGANIZATION R & D Associates 6b. OFFICE SYMBOL (If applicable)	7a. NAME OF MONITORING ORGANIZATION Director Defense Nuclear Agency
6c. ADDRESS (City, State and ZIP Code) 1401 Wilson Blvd. Arlington, VA 22209-2381	7b. ADDRESS (City, State and ZIP Code) Washington, DC 20305-1000
8a. NAME OF FUNDING/SPONSORING ORGANIZATION 8b. OFFICE SYMBOL (If applicable)	9. PROCUREMENT INSTRUMENT IDENTIFICATION NUMBER DNA 001-85-C-0025
8c. ADDRESS (City, State and ZIP Code)	10. SOURCE OF FUNDING NUMBERS PROGRAM ELEMENT NO. 62715H; PROJECT NO. Y99QMXS; TASK NO. C; WORK UNIT ACCESSION NO. DH008686

11. TITLE (Include Security Classification)
SUMMARY OF DIHEST SIMULATOR EXPERIMENTS AND EFFORTS IN SUPPORT OF THE ADVANCED SILO HARDENING PROGRAM

12. PERSONAL AUTHOR(S)
Webster, J. Burton, III, Ph.D.

13a. TYPE OF REPORT	13b. TIME COVERED	14. DATE OF REPORT (Year, Month, Day)	15. PAGE COUNT
Technical Report	FROM 840101 TO 841231	850301	

16. SUPPLEMENTARY NOTATION
This work was sponsored by the Defense Nuclear Agency under RDT&E RMSS Code B341085466 Y99QMXSC00041 H259OD.

17. COSATI CODES			18. SUBJECT TERMS (Continue on reverse if necessary and identify by block number)
FIELD	GROUP	SUB-GROUP	
19	4		Ground Shock, DIHEST Data
14	2		DIHEST High Explosive Simulation,
			DIHEST Predictive Methods,

19. ABSTRACT (Continue on reverse if necessary and identify by block number)

This report summarizes the results of efforts by the DNA Ground Shock Simulation community to develop design techniques and predictive methods for producing crater related motions using the Direct Induced High Explosive Simulation Techniques (DIHEST). The work was performed by several investigators under the sponsorship of DNA, and was subjected to review and comment in the forum of the Advanced Silo Hardening (ASH) Simulation Working Group. The report briefly presents the evolutionary steps involved in reading improved predictive methods, and the relationships for those methods are re-developed. A summary of the DIHEST data used during the development along with recent experimental data are provided along with some comments on the applicability of prior experiments.

20. DISTRIBUTION/AVAILABILITY OF ABSTRACT	21. ABSTRACT SECURITY CLASSIFICATION
☐ UNCLASSIFIED/UNLIMITED ☒ SAME AS RPT. ☐ DTIC USERS	UNCLASSIFIED

22a. NAME OF RESPONSIBLE INDIVIDUAL	22b. TELEPHONE (Include Area Code)	22c. OFFICE SYMBOL
Betty L. Fox	(202) 325-7042	DNA/STTI

DD FORM 1473, 84 MAR 83 APR edition may be used until exhausted.
All other editions are obsolete.

UNCLASSIFIED
SECURITY CLASSIFICATION OF THIS PAGE

TABLE OF CONTENTS

List of Illustrations

List of Tables

SECTION 1
INTRODUCTION

When DNA and BMO entered into a joint program to test the hardness of superhard silo designs as a basing candidate for the Small ICBM, it was apparent that nuclear airblast and groundshock methods would have to be extended and modified. Proximity to the burst point would be much closer than in any prior test programs. One of the principal motion categories was the ground motions directly induced by the cratering mechanics for a surface burst. DNA formed a Simulation Working Group to support the Integrated Superhard Silo Test (ISST) program, and one of its principal goals was to oversee the development of the direct induced motion simulation designs. This report deals with progress made during 1984 towards understanding the performance of a simulation technique called DIHEST for producing direct induced motions using high explosive placed in a vertical drill hole array. The year's efforts were focussed on understanding planar charge arrays which were not influenced by added motions from the simulation of airblast loading on the surface. Combined surface and direct induced motions were the subject of the FY85 program.

The DIHEST simulation methodology has been developed over a fairly broad time span, and the data have been reported in a number of test reports and data compilations. The most recent comprehensive review was performed by C.J. Higgins, et. al., in a three volume report from an earthquake simulation program sponsored by the National Science Foundation[1]. A follow-on to that effort was sponsored by the Electric Power Research Institute[2,3]. Six DIHEST arrays were exploded in three test events (pairs of arrays were detonated for each test). Those tests, designated Mini SIMQUAKE, SIMQUAKE I and SIMQUAKE II, were conducted at the McCormick Ranch test site

south of Albuquerque. Layouts are shown from References 2 and 3 at Figures 1, 2, and 3.

Prior to the SIMQUAKE tests, there were two other DIHEST development test series conducted at the McCormick Ranch site: the DIHEST Enhancement Program (DEP), and the DIHEST Improvement Program (DIP). The DEP series consisted of 13 tests which included four planar array tests (See Table 1 excerpted from Higgins in Reference 1). Note that shots 9 and 13 both involved boundary relief experiments. Shot 9 had a relief trench on one side of the array, and peak quantities measured from the other side should not have been affected. However, shot 13 had a boundary relief trench on one side, and three rows of 3-foot diameter holes drilled on the other side of the array. Therefore, the peak quantities are probably suspect with respect to shot 13 when trying to obtain correlation with other experiments which had no such relief designs. The configurations shown by Higgins[1] are at Figure 4.

The DIHEST Improvement Program had three planar shots (See Table 2). Note that DIP III A was a boundary relief experiment similar to DEP Shot 13. Test bed layouts for the planar DIP tests are at Figures 5, 6, and 7. One other large DIHEST test, named ACID, was fired at McCormick Ranch.

A data base was built for the Apple Lisa computer spreadsheet. The SIMQUAKE, DEP, DIP, and ACID data were obtained from C.J. Higgins and Jim Drake of Applied Research Associates, Inc. (ARA). The data base will be expanded as data becomes available from the WES tests of YUMA and the AFWL/NMERI DIHEST Development tests (DDT) at McCormick Ranch. The spreadsheet software is particularly useful when used with the Lisa graphics plotter package to view the results

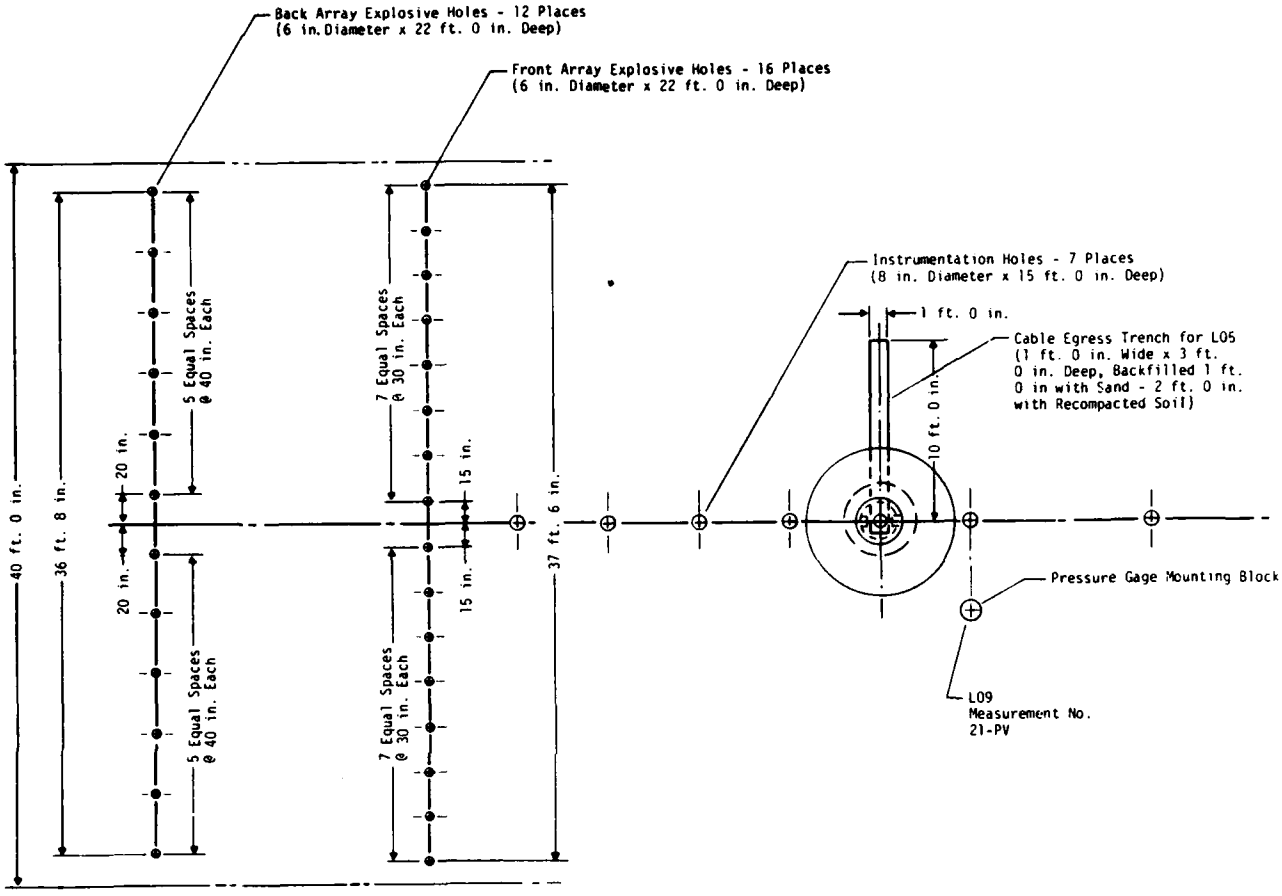

Figure 1. Mini-SIMQUAKE - test bed layout.

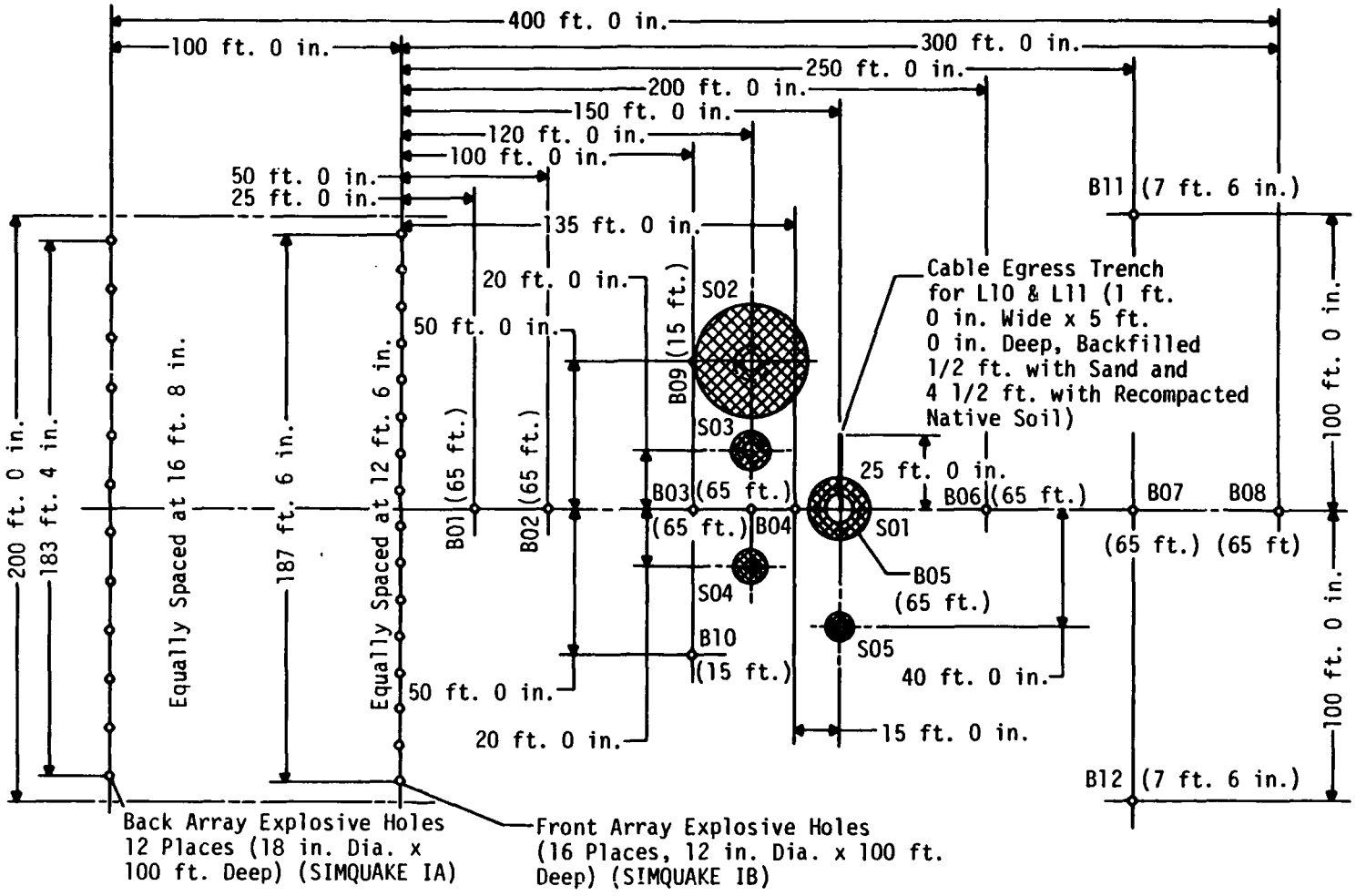

Figure 2, SIMQUAKE I - test bed layout.

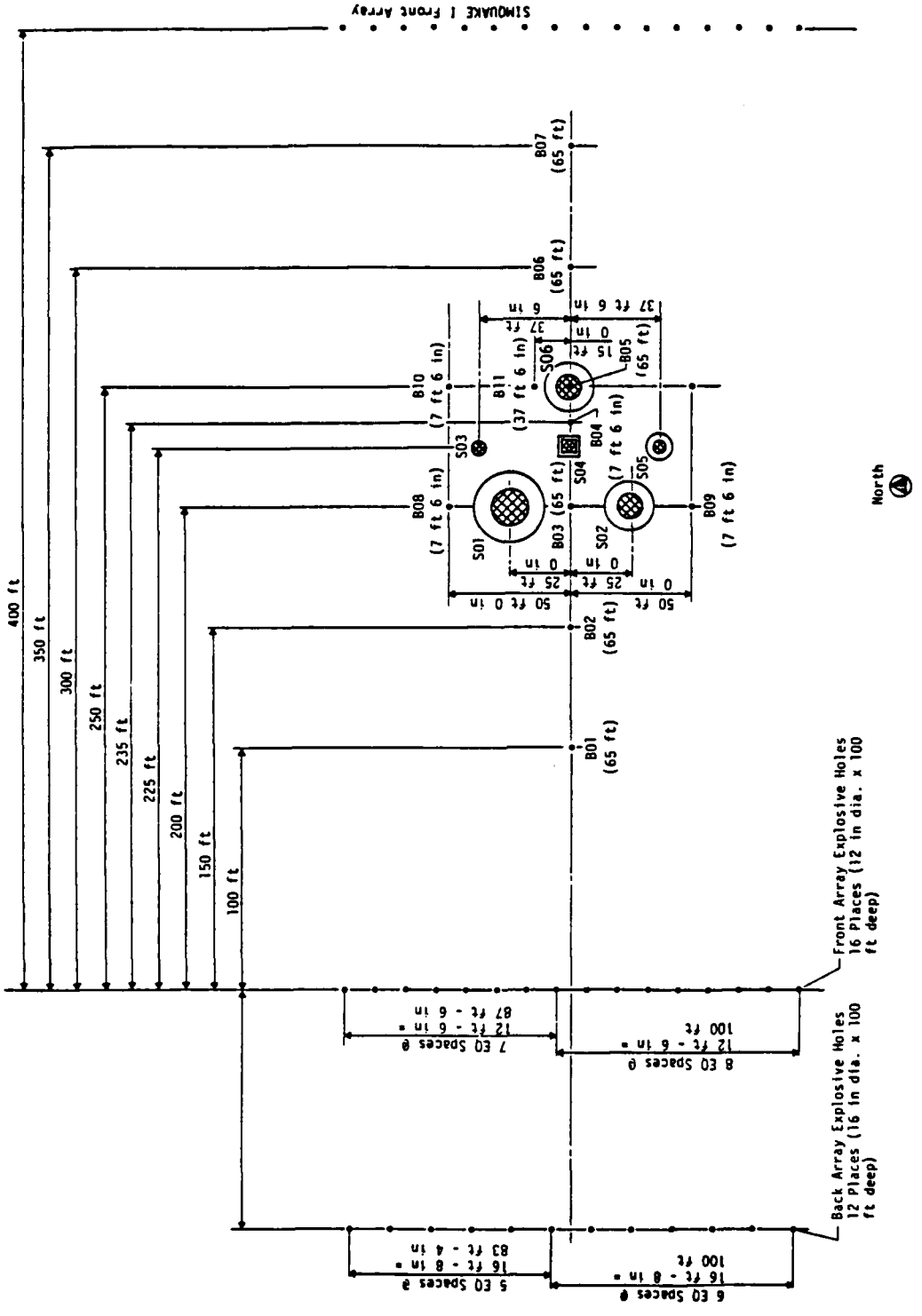

Figure 3. SIMQUAKE II - test bed layout.

Table 1. DIHEST enhancement program; explosive placement, geometry and array parameters.

Shot #	Explosive Array	ARRAY GEOMETRY					EXPLOSIVES					OBJECTIVES
					Array Details				Placement	Density		
		L ft.	H ft.	S ft.	Arc Angle degrees	R ft.	Type	W lbs	N Holes	α lbs/ft^2	γ lbs/ft	
1	Planar	12	4	4	-	-	PETN	48	C	1	*	Focusing (1 vs 2)
2	V-Shape	12	4	4	60	-	PETN	48	C	1	-	Focusing (1 vs 2)
3	Planar	20	6.7	6	-	-	PETN	133	16	1	(1.24)	Focusing (3 vs 4,5)
4	Curved	20	6.7	6	120	9.5	PETN	133	16	1	(1.24)	Focusing (3 vs 4)
5	Curved	20	6.7	6	120	9.5	PETN	133	16	1	(1.24)	Repeat of 4
6	Cylindrical	-	12.	6	-	-	PETN	60	1	-	5	Decoupling (6,7 and 8)
7	Cylindrical	-	12.	6	-	-	PETN	60	1	-	5	Decoupling (6,7 and 8)
8	Cylindrical	-	12.	6	-	-	PETN	60	1	-	5	Coupling (6,7 and 8)
9	Planar	40	13.3	8	-	-	PETN	2133	11	4	(14.5)	Relief (9A vs 9B)
10	Curved	40	13.3	8	120	19	PETN	2133	11	4	(14.5)	Focusing (9A vs 10)
11	Curved	40	13.3	8	120	19	PETN	2133	7	4	(22.9)	Decoupl.in Arr.(10 vs 11)
12	Cylindrical	-	13.3	8	-	-	PETN	305	1	-	22.9	Yield Variation(12 vs 6,7)
13	Planar	40	13.3	8	-	-	PETN	533	11	1	(3.6)	Relief Variation(9 vs 13)

NOTES: 1. Figures in ( ), indicate equivalent line (cylindrical) charge per drill-hole

2. C indicates continuous charge density in a trench configuration.

3. Symbols: L = array length, H = array height, S = height of surcharge above explosive, W = explosive weight, α = areal charge density in two dimensional array, γ = line charge density in cylindrical charge, R = radius of curved array

* Absence of a value for γ indicates explosive was distributed uniformly in a trench.

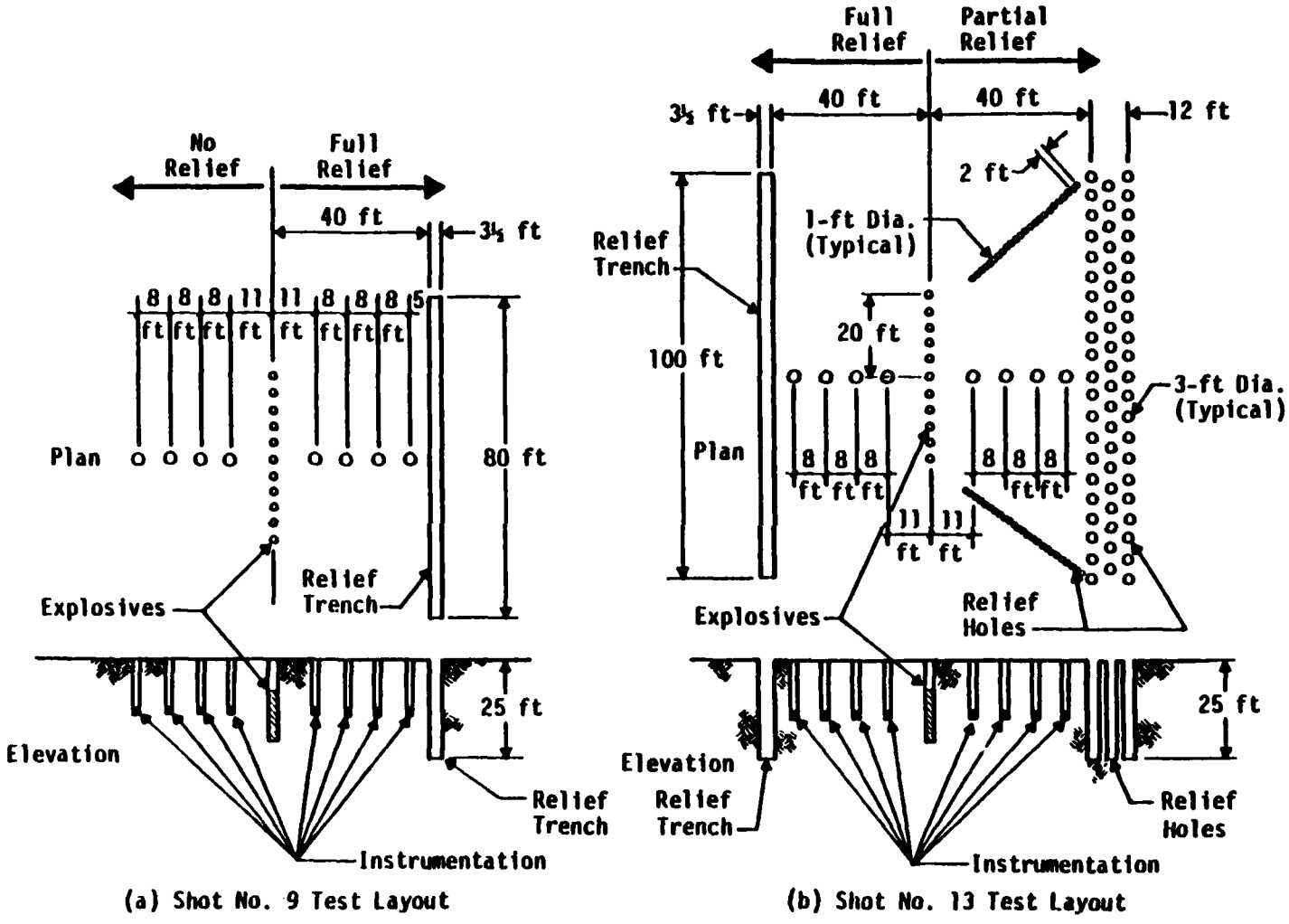

Figure 4. Configurations of the boundary relief experiments.

Table 2. Parameters for large soil DIHEST events.

Event	Array Type	ARRAY GEOMETRY L ft	H ft	S ft	EXPLOSIVES Type	W Tons	No. of Holes	Density ρ lbs/ft³	Density γ lbs/ft	Remarks	Reference
DIP IA	Concentrated Charge	-	-	40*	DBA-22M Slurry	40	-	-	-	Large concentrated charge	II-10
DIP IIA	Planar Array	208	35	30	DBA-22M Slurry	40	29	11.4	(78.8)	Largest charge density array	II-11
DIP IIIA	Planar Array	107.5	33	20	DBA-22M Slurry	3.3	15	1.86	(13.33)	Boundary relief Experiment	II-12
DIP IVA	Concentrated Charge	-	-	10.75*	DBA-22M Slurry	0.5	-	-	-	Small concentrated charge	II-13
DIP VA	Planar Array	1134	204	30	6ST2 Slurry	40	16	0.35	(24.6)	Largest size array smallest charge density	II-13

* Depth to center of concentrated charge

Notes and nomenclature are the same as for table 1

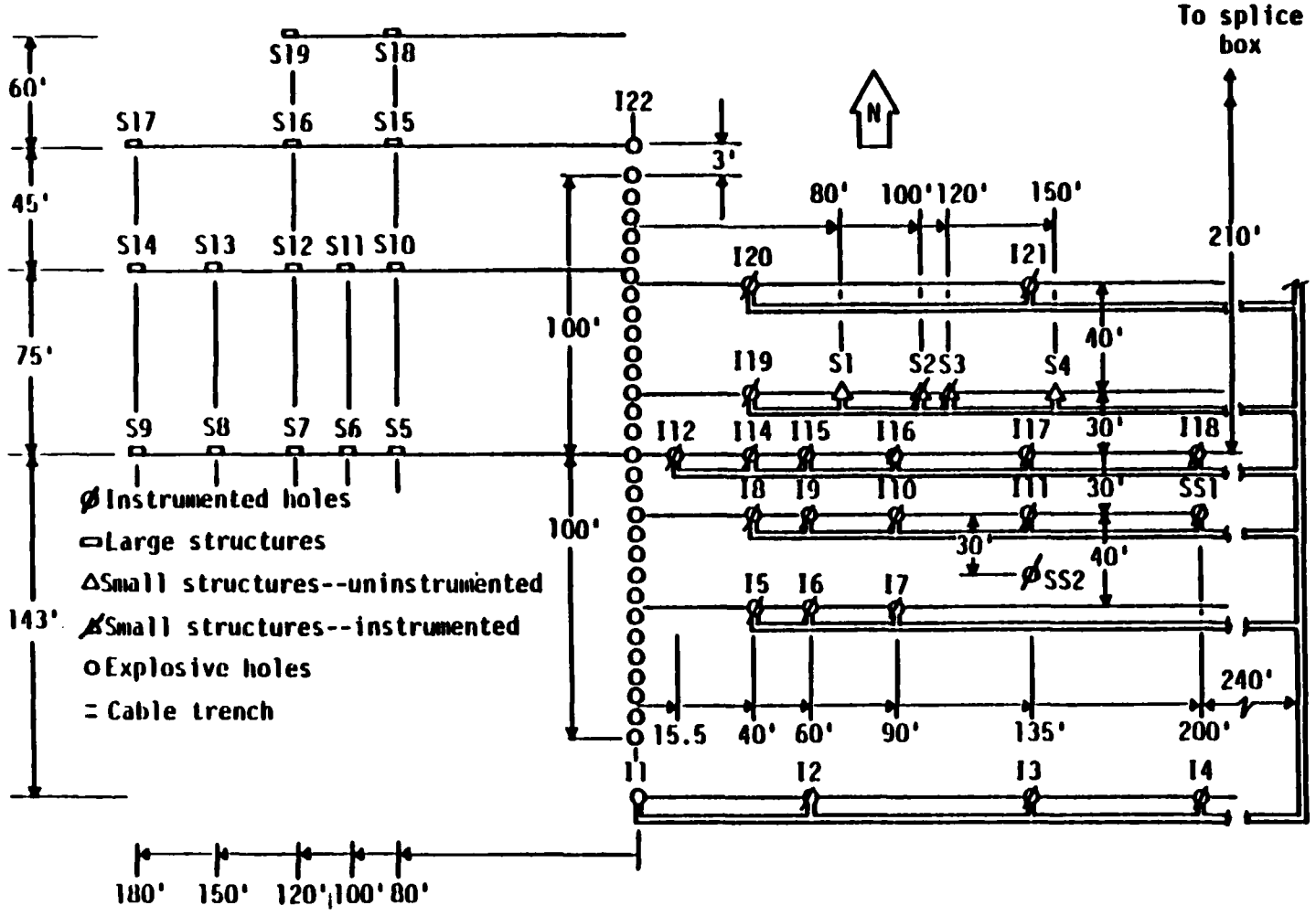

Figure 5. DIP IIA - test bed layout.

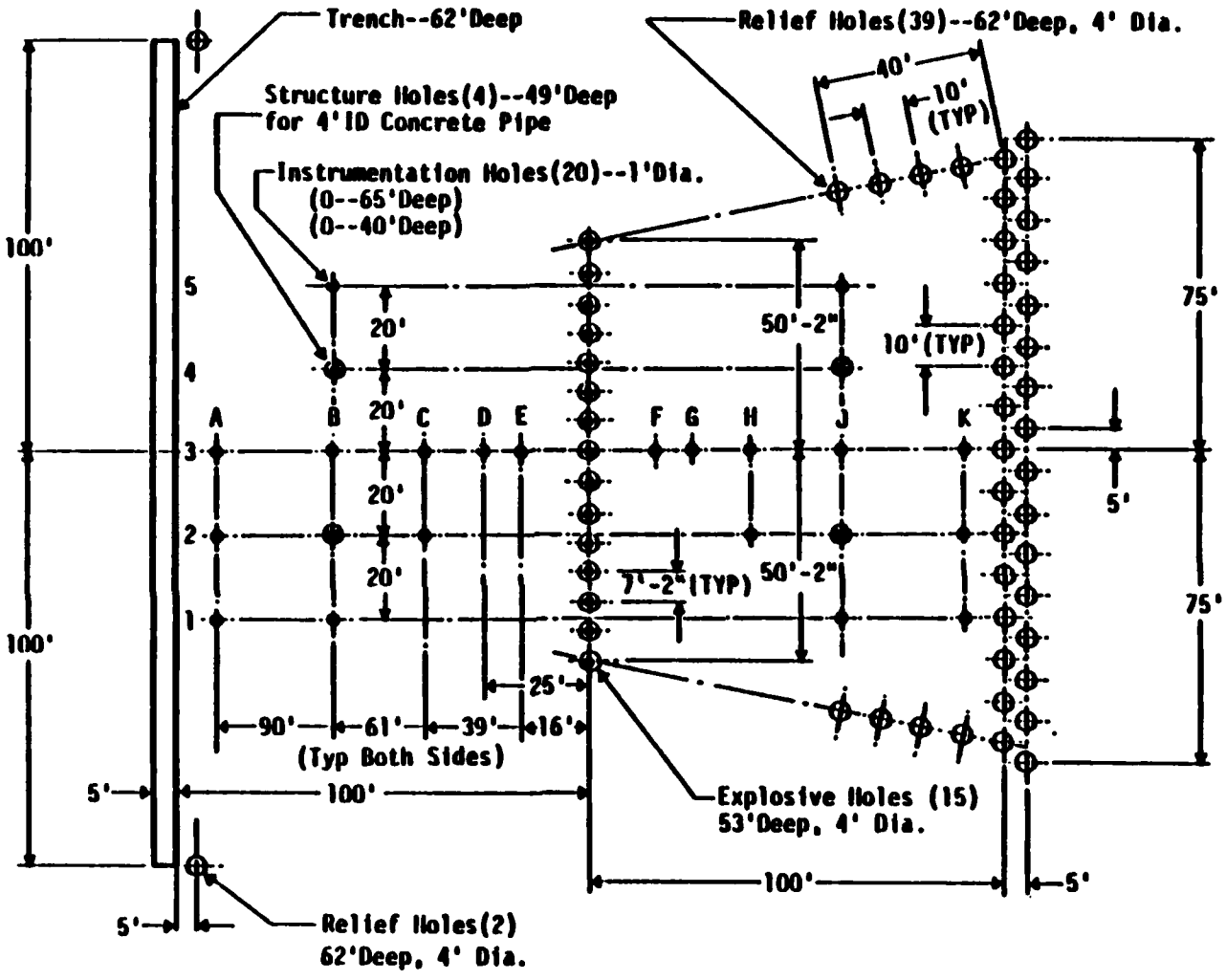

Figure 6. DIP IIIA layout.

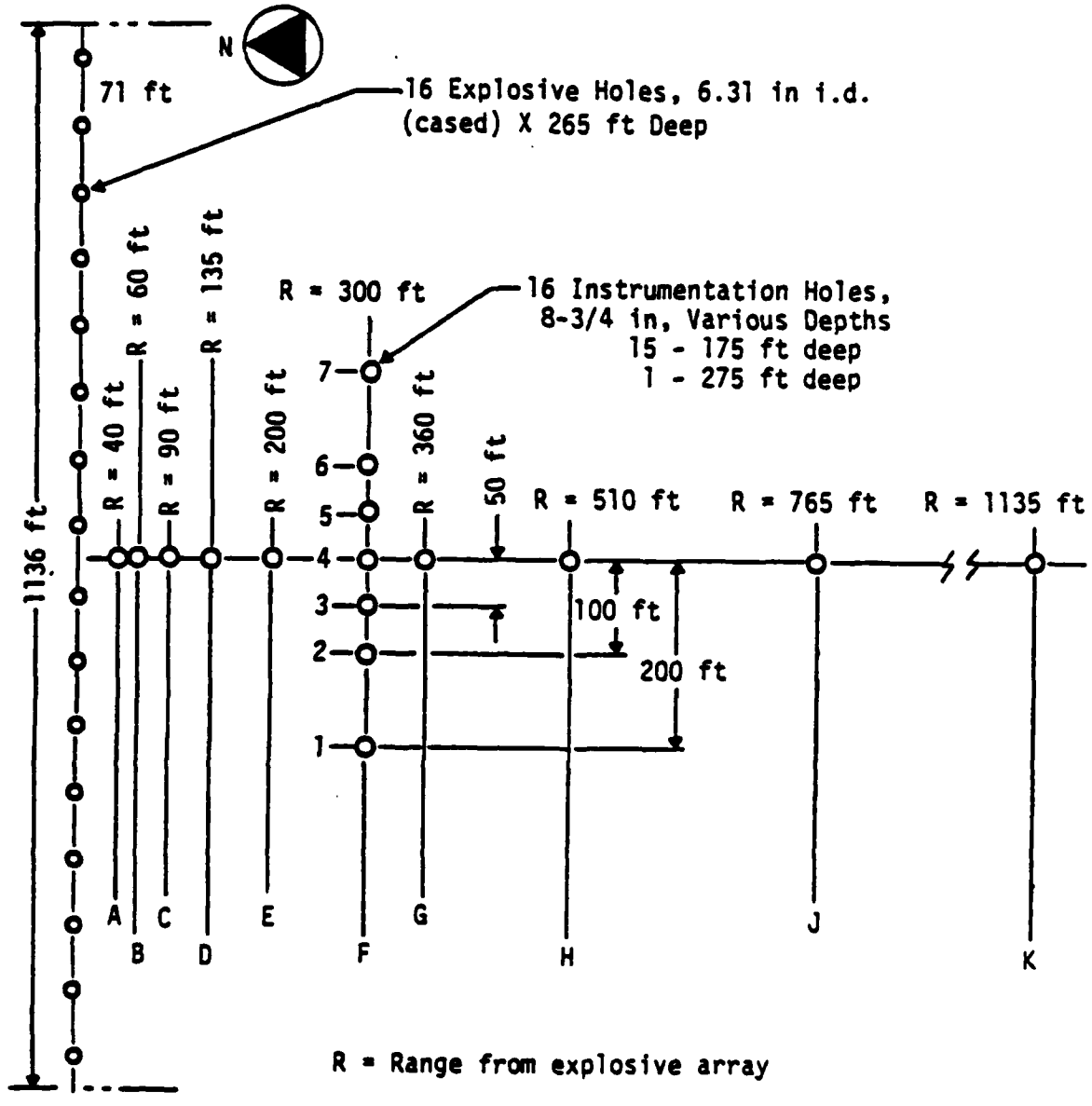

Figure 7. DIP VA - test bed layout.

of data collapsing methods. To standardize data presentations, the following testbed design nomenclature was used to describe the parameters shown in Figure 8.

H - array charge height
L - array length
b - burial depth from top of ground or surcharge surface to the top of the charge array
D - explosive hole diameter
s - spacing of charge holes
n - number of charge rows
Sr - spacing between charge rows
α - areal charge density in terms of equivalent weight of TNT per unit array area

The remainder of this report presents the results of several approaches used to provide predictive relationships for *DIHEST* designs. First, the pre-existing design equations are presented along with a brief discussion of the shortcomings discovered during early examinations under the ISST program. Then a chronological development of the two more recent correlations follows.

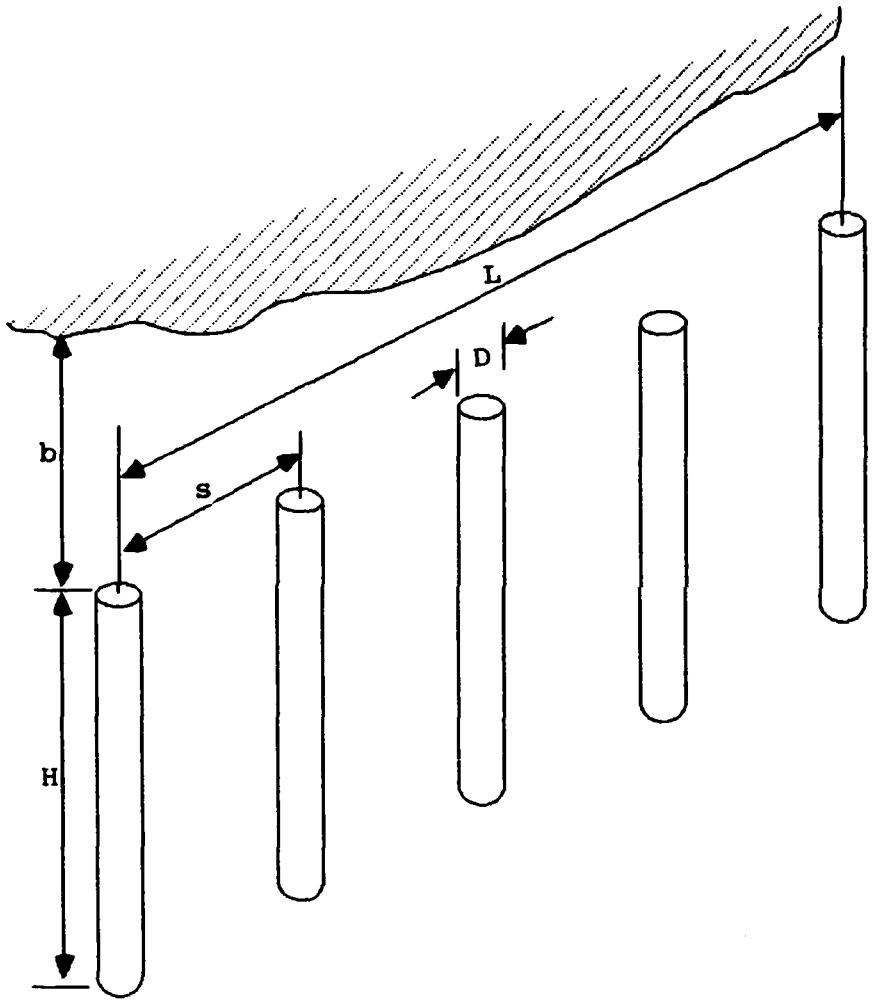

D - hole diameter
b - burial depth
s - hole spacing
H - charge height
L - array length
N - number of charge rows
Sr - charge row spacing
α - equivalent TNT weight per unit area (lbs/ft**2)

Figure 8. DIHEST array parameters.

SECTION 2
PREDICTIVE METHODS

Higgins Method. The majority of the DIHEST events had array aspect ratios (length to height) of around 3:1. Predictive methods (data correlations) generally ignored array length and considered only the height. This was also the case for most calculational predictions, since generally these were made using 2-D plane strain hydrocodes which assumed an infinite array length. The principal dynamic variables (acceleration, velocity, and displacement) were cast in predictive relationships which depend upon range, areal charge density, and array height. Higgins presented the following relationships for peak values of horizontal acceleration, particle velocity, and displacement at the depth of the array centerline for the McCormick Ranch planar events:

$$a^{*}\alpha = \begin{cases} 10{,}150\,(R/\alpha)^{-1.33} & R/H \le 0.52 \quad (1\text{-a}) \\ 4119\,(H/\alpha)^{1.38}\,(R/\alpha)^{-2.71} & R/H > 0.52 \quad (1\text{-b}) \end{cases}$$

$$v = \begin{cases} 81.8\,(R/\alpha)^{-0.56} & R/H \le 1.15 \quad (2\text{-a}) \\ 101.4\,(H/\alpha)^{1.54}\,(R/\alpha)^{-2.1} & R/H > 1.15 \quad (2\text{-b}) \end{cases}$$

$$d/\alpha = \begin{cases} 4.6\,(R/\alpha)^{-0.14} & R/H \le 1.6 \quad (3\text{-a}) \\ 11.7\,(H/\alpha)^{1.96}\,(R/\alpha)^{-2.1} & R/H > 1.5 \quad (3\text{-b}) \end{cases}$$

where the parameters are defined as:

a = acceleration in g's
v = velocity in ft/sec
D = displacement in inches
R = range in feet
H = array height
α = areal charge density (lbs TNT/ft^2)

These relationships are good representations of the data available for the McCormick Ranch test site, and even the DIP IIA and DIP VA tests which had array aspect ratios of about 6:1 don't diverge greatly from the test of the data. However, when the two 1:1 aspect ratio (WES 1 and WES 4) tests were shot, the peak values fell well below the predictions made without considering array length. These tests demanded a re-examination of the DIHEST design relationships.

A joint collaboration between ARA, RDA and CRT under the sponsorship of the DNA ASH program led to a re-examination of the DIHEST data. To present the new formulations, a stepwise development is presented here which approximates the process followed to derive them.

Evidence for Array Length Dependence. At a Working Group on 8 February 1984, Jim Drake of ARA presented an approach which did a better job of collapsing the available data (Ref. 4). He normalized the distance from the array to the measurement point by the array height vice the areal charge density used by Higgins and others. His method was to plot the kinematic variables (velocity, product of acceleration and charge density, and displacement divided by charge density) against the range reduced by the array height. He found generally that a log-log plot of velocity vs R/H would be described by a straight line of slope minus 2. By plotting the logarithm of the value of V at the intercept (R/H = 1) versus the logarithm of H/α , he found that a linear relationship would generally fit that dependence as well. However, when the data for the first two WES shots at Yuma were treated this way, they were decidedly not on the same line as the previous data. Figure 9 shows all of the data discussed along with the first of the AFWL DIHEST Development Tests (DDT-1) which had an array aspect ratio of 1.6:1. The intercept of

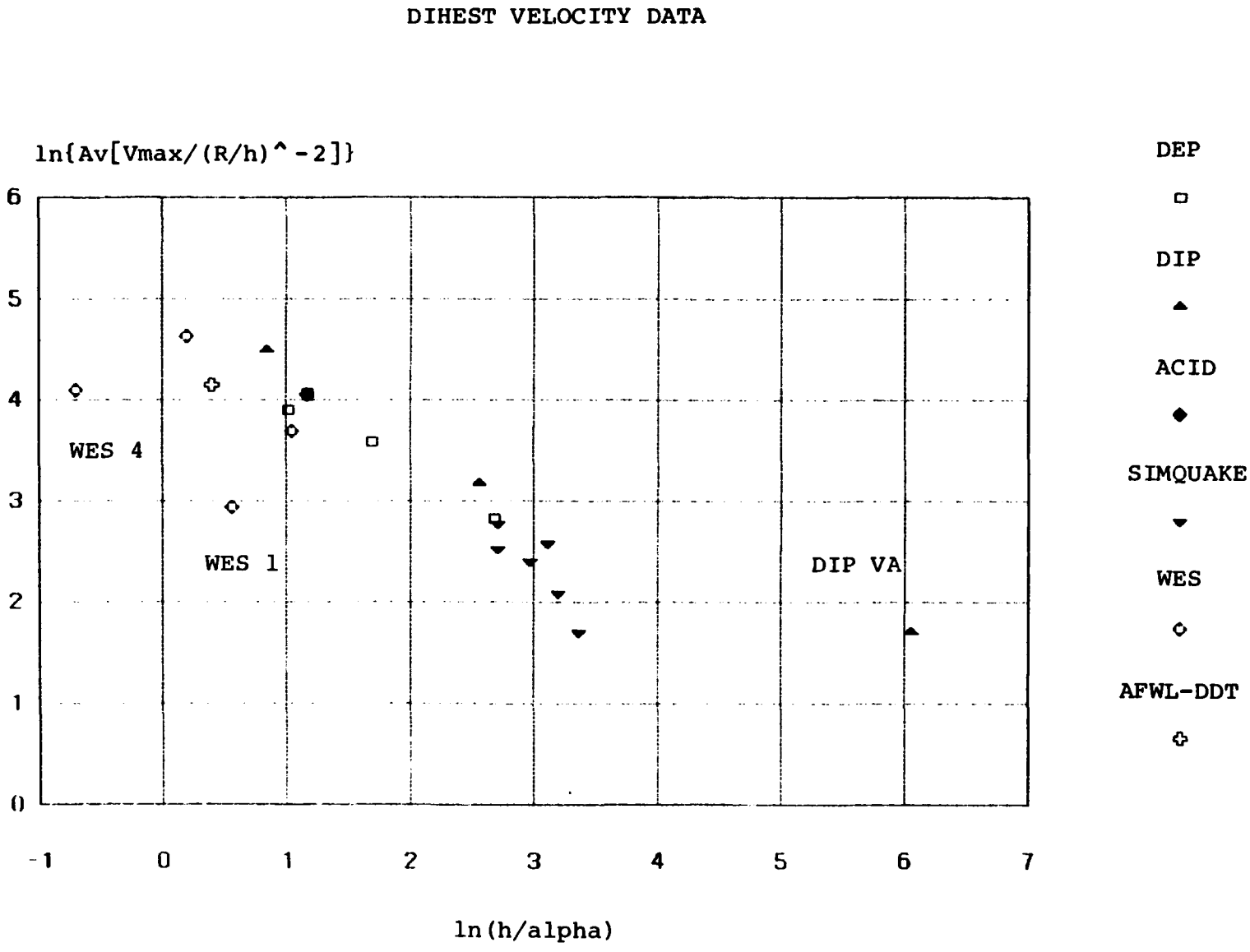

Figure 9. DIHEST velocity corollation using normalized array height.

the peak velocity shows a definite dependence upon the aspect ratio. This intercept for a given test is really just the average value of V_{max} reduced by the factor $(H/R)^2$. The WES tests (aspect ratio, Ar = 1.1) fall well to the left of the other data. The AFWL-DDT test (Ar = 1.6) is nearer the main body of data, but still on the left edge. The SIMQUAKE events (Ar = 2.67) and the DEP and ACID events (Ar = 3.0) fall generally together. Finally, DIP IIA and DIP VA (Ar = 6) fall to the right of the rest of the data.

Effective Array Length Correlation. Our first attempt to account for the aspect ratio dependence was to include a dimensionless term, $(L/H)^m$ in the relationship. The problem with this approach is that unless m along with the powers of the terms R/H and H/α are exactly proportioned, the relationship would not be symmetric in L and H. Thus, an array whose aspect ratio is less than 1 could not be characterized by simply swapping L and H for an array whose aspect ratio is the inverse. The form of the relationship was viewed as having definite limitations.

Fred Sauer, CRT, suggested that the influence of the top, bottom, and ends of the array can be viewed as having diminishing strength the farther they are removed from the centerline relative to one another. This is somewhat analogous to the influence of parallel resistors in an electrical circuit. He therefore suggested that in place of the array height an "effective length" based upon the inverse of the sum of the inverses of length and height be assessed for the predictive relationships. This was approached by essentially following Higgin's procedure: reducing the range by the areal charge density, and then using the ratio of the effective length (defined by the inverse of the sum of the inverse lengths to the centerline from the top and ends of the array)

to the areal charge density to obtain a relationship which is symmetric in L and H. Defining this effective length, LN, as

$$LN = \frac{1}{1/(2*H) + 1/(2*L)} = \frac{2*L*H}{L + H} \qquad (4)$$

the data were re-analyzed. The data used for this analysis are found in Appendix A, and are organized by the test series. Because of its similarity to the other planar array tests in the DIP series, ACID data was grouped with data from DIP. This analysis was done by using the features of the Lisa spreadsheet software. First, the chosen kinematic variable was reduced by the quotient of the range divided by the areal charge density. The intercept value (at $R/\alpha = 1$) was found by simply taking the average of those values. The data from each event were examined, and some of the points were excluded from the fits. Exclusion was based upon the judgement, in collaboration with Drake[6], that the data records exhibited questionable behavior, and would make the fits less useful for predictive purposes. Those points were noted on the spreadsheet with an asterisk (*). These spreadsheets are contained in the Appendix B. These intercepts were plotted against Ln/α as they appear in Figure 10 for the velocity, Figure 11 for d/α, and Figure 12 for $a^*\alpha$.

The efficiency of using the effective length variable, LN, is best judged by examining Figures 10 through 12. The WES data exhibit some variance which may be due to the different material at the YUMA site, but the McCormick Ranch data correlate very well.

Least squares fits were made for the kinematic variables, but the data for the two WES events, DEP shot 13 and DIP IIIA were excluded. It should be noted that the exclusion of DEP shot 13 and DIP IIIA did not significantly change the fits, so the partial boundary relief may not have had a

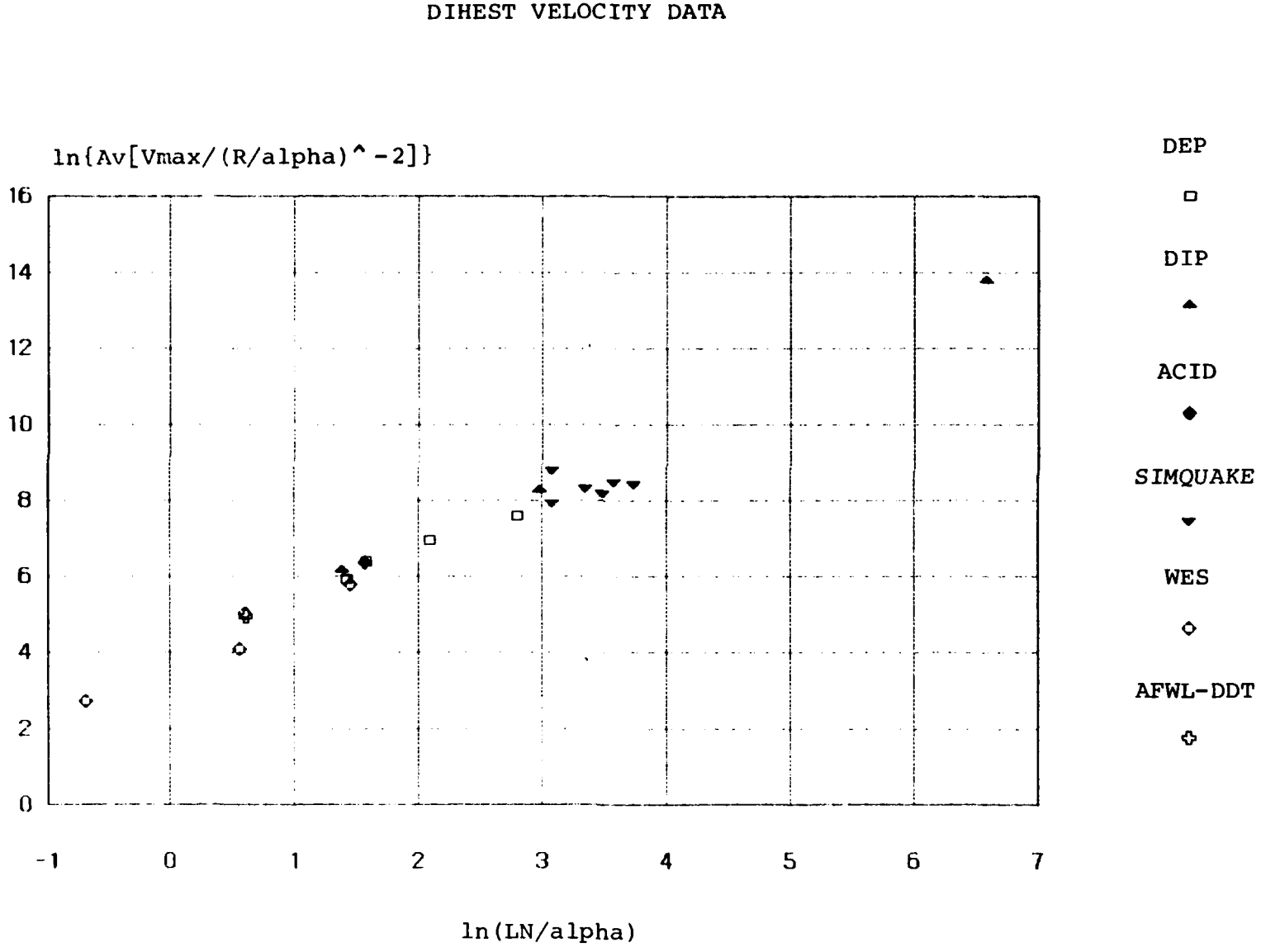

Figure 10. DIHEST velocity corollation using effective length.

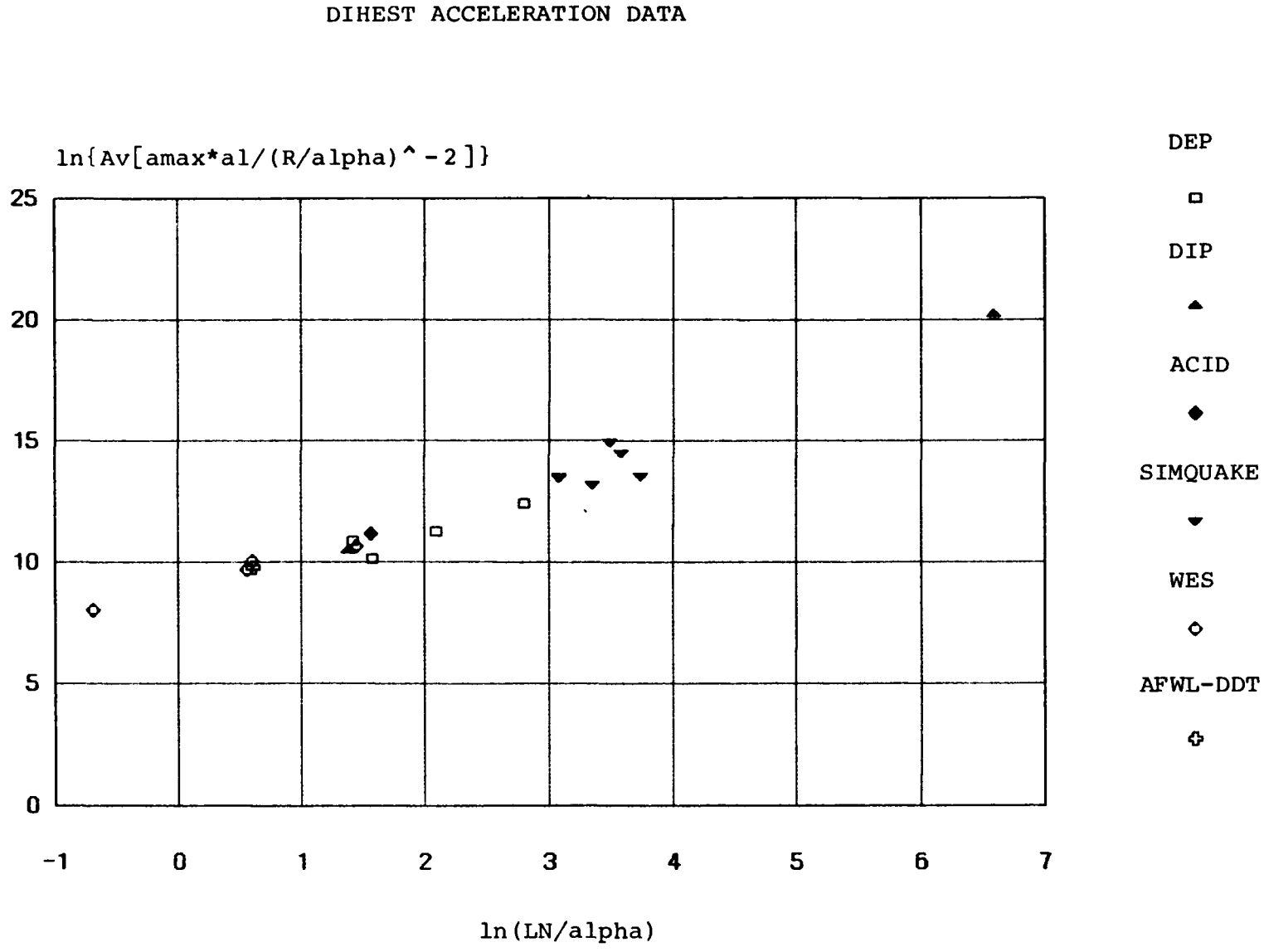

Figure 11. DIHEST acceleration corollation using effective length.

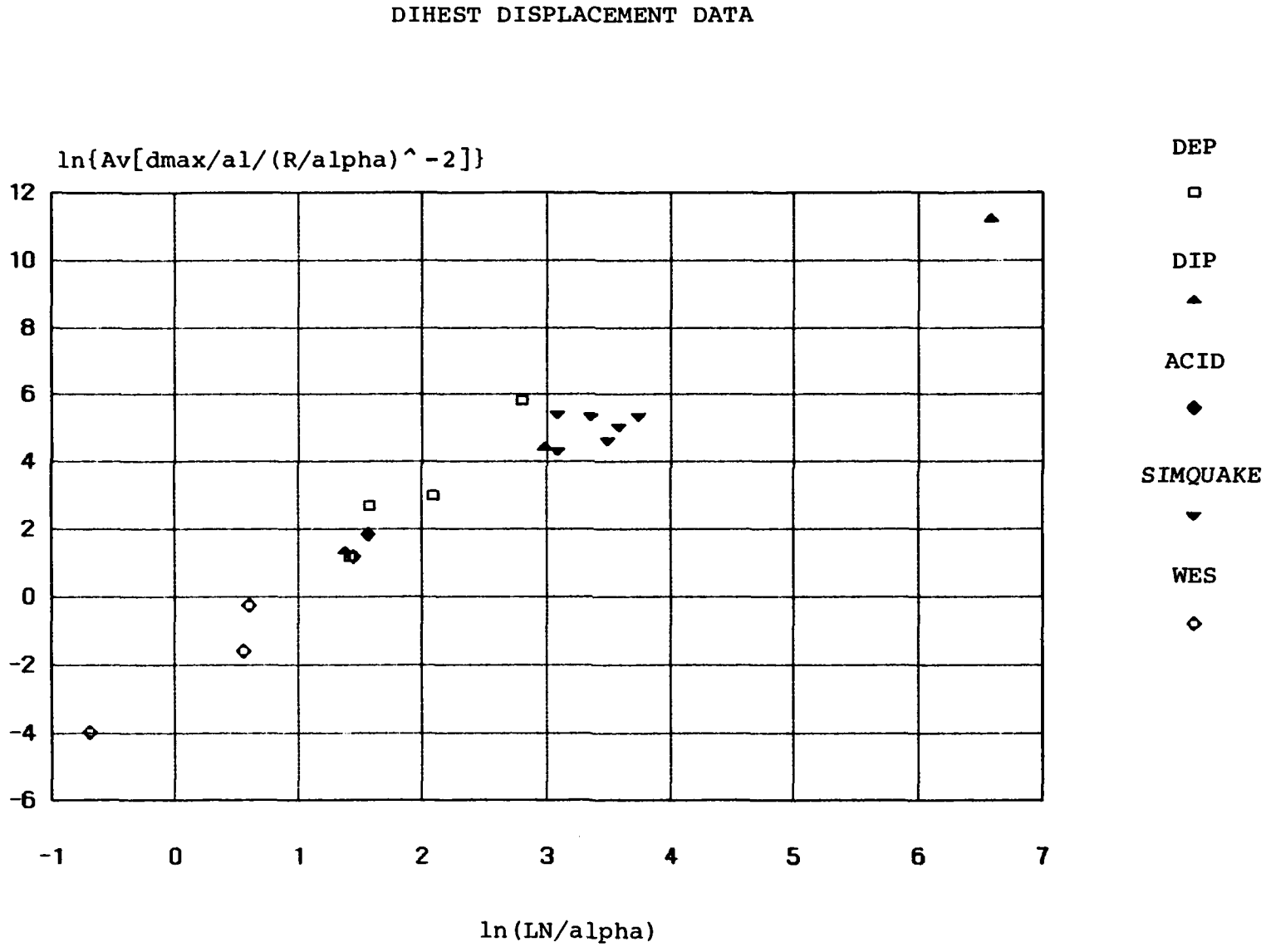

Figure 12. DIHEST displacement corollation using effective length.

significant effect upon the peak values. Integer powers were chosen for the dependence upon the ratio of R/α. The relationships obtained were:

$$a*\alpha = 3020(LN/\alpha)^{1.8}(R/\alpha)^{-3} \quad (5)$$

$$V = 53(LN/\alpha)^{1.38}(R/\alpha)^{-2} \quad (6)$$

$$d/\alpha = 0.45(LN/\alpha)^{1.8}(R/\alpha)^{-2} \quad (7)$$

ADDITIONAL OBSERVATIONS. Some additional insight into the form of the velocity equation may be gained by breaking the equation down by its individual parameters as:

$$V = 53*[2Ar/(1 + Ar)]^{1.38} * H^{1.38} * \alpha^{0.62} * R^{-2}. \quad (8)$$

Suppose that the power of (LN/α) were constrained to be 4/3 (1.33 instead of 1.38), then

$$V = 61*[2Ar/(1 + Ar)]^{4/3} * (H^2*\alpha)^{2/3} * R^{-2}. \quad (9)$$

Since the total charge weight, W is given by

$$W = \alpha*HL = \alpha*Ar*H^2, \quad (10)$$

equation 9 can be written as

$$V = 61*[4Ar/(1 + Ar)^2]^{2/3}*(Ar*H^2*\alpha)^{2/3}*R^{-2} \quad (11)$$

or,

$$V = 61*[4Ar/(1 + Ar)^2]^{2/3}*(R/W^{1/3})^{-2} \quad (12)$$

Thus the form contains a dependence on the range reduced by the cube root of the charge weight and a specific

function of the aspect ratio. That function indicates that for a given charge weight, at a given range, an aspect ratio of _ gives the maximum velocity. However, the acceleration and displacement requirements must be considered when selecting a specific DIHEST design. The next step then was to see if a natural dependence on the charge weight was evident in the fits for acceleration and displacement.

If the coefficient value 1.8 in equation 5 were constrained to be 2.0, then equation 5 for the accelerations could be cast in a form similar to equation 12 as:

$$a^{*}\alpha = 1590[4Ar/(1 + Ar)^{2}]*(R/W^{1/3})^{-3} \qquad (13)$$

This form shows a definite dependence upon the charge weight and array aspect ratio. Even the general form of the equation is in agreement with that of equation 12. However, when the displacement equation is subjected to similar treatment, the dependence is apparent, but the form is somewhat different. If the coefficient 1.8 in equation 7 for the displacement were replaced by 2.0, the equation could be rearranged as:

$$d/\alpha = 0.2*(LN/W^{1/3})^{2}*(R/W^{1/3})^{-2} \qquad (14)$$

Here the effective length term is also reduced by the cube-root of the charge weight. For the velocity and acceleration relationships this term was of the form $(LN^{2}*\alpha/W^{1/3})^{n}$, and reduced to a non-dimensional function of aspect ratio. The lack of consistency for scaling the displacement relationship when compared with the other kinematic parameters suggested that the use of a reduced length may not be general enough to adequately describe the data.

SECTION 3
CONSISTENT SCALING

Once the simple cube-root of charge correlation was identified, Jim Drake extended the idea to better describe the physical situation of finite arrays. This section presents a brief summary of Drake's approach.[5] He developed a set of predictive expressions which are dimensionally consistent and describe peak motions along the array centerline in terms of regions whose attenuation is characterized as planar, cylindrical, or spherical.

Planar attenuation occurs in the region nearest the charge array where the array sides do not influence the peak motion parameters. The term cylindrical attenuation is used to characterize the region where the shortest array dimension (normally the height for most DIHEST arrays) influences attenuation after the fashion of a line charge of explosive. Spherical attenuation characterizes the region farthest away from the charge where all sides of the array influence attenuation, approaching the behavior of a point charge.

To derive his predictive expressions, Drake required that they be continuous at region boundaries, reduce to the canonical scaling form for each region, and be symmetric with respect to array height and length. The canonical scaling form for any region may be generally written for the motion parameters as:

$$a\Phi_i = A_i(R/\Phi_i)^{-m_i}$$

$$v = V_i(R/\Phi_i)^{-n_i} \qquad (15)$$

$$d/\Phi = D_i(R/\Phi_i)^{-n_i}$$

where Φ_i is the appropriate array parameter for the i^{th} region; A_i, V_i and D_i are regional coefficients of the fit; and m_i, n_i and p_i are the regional attenuation coefficients. The array parameters for each region are:

Region	Φ
planar	α
cylindrical	$\gamma^{1/2}$
spherical	$W^{1/3}$

The parameters are simply related through the expressions:

$$\begin{aligned} \gamma &= \alpha H \\ W &= \alpha HL = \gamma L \end{aligned} \tag{16}$$

The forms chosen for the expressions in the three regions were:

$$a*\alpha = \begin{cases} a_o (\alpha/R)^i & R < fH \\ a_o (\alpha/R)^i \, (fH/R)^j & fH \le R < fL \\ a_o (\alpha/R)^i \, (fH/R)^j \, (fL/R)^j & fL \le R \end{cases}$$

$$v = \begin{cases} v_o (\alpha/R)^k & R < fH \\ v_o (\alpha/R)^k \, (fH/R)^l & fH \le R < fL \\ v_o (\alpha/R)^k \, (fH/R)^l \, (fL/R)^l & fL \le R \end{cases}$$

$$d/\alpha = \begin{cases} d_o (\alpha/R)^m & R < fH \\ d_o (\alpha/R)^m \, (fH/R)^n & fH \le R < fL \\ d_o (\alpha/R)^m \, (fH/R)^n \, (fL/R)^n & fL \le R \end{cases}$$

Here f is some fraction of the array height or length where that boundary begins to affect centerline motion. Thus, the planar region extends to a range of fH, and the cylindrical region ends at a range of fL for an array whose length is

greater than its height. For the expressions to reduce to the canonical form of equation 15, Drake found that the exponents had to conform to the following relationships:

$$\begin{aligned} i &= j + 1 \\ k &= 1 \\ m &= n - 1 \end{aligned} \qquad (17)$$

Based upon examination of the available data, Drake chose the value of f to be 0.5, noting that the fits were not strongly dependent upon the choice of f since the transition between regions was not a sharp one. Drake performed least squares fits to the data available in each region, and recommends the following expressions for predicting peak motions along the centerline of a DIHEST:

$$a * \alpha = \begin{cases} 15{,}835(\alpha/R)^{5/3} & R < H/2 \\ 15{,}835(\alpha/R)^{5/3}\,(H/2R)^{2/3} & H/2 \le R < L/2 \\ 15{,}835(\alpha/R)^{5/3}\,(H/2R)^{2/3}\,(L/2R)^{2/3} & L/2 \le R \end{cases}$$

$$v = \begin{cases} 123(\alpha/R)^{2/3} & R < H/2 \\ 123(\alpha/R)^{2/3}\,(H/2R)^{2/3} & H/2 \le R < L/2 \\ 123(\alpha/R)^{2/3}\,(H/2R)^{2/3}\,(L/2R)^{2/3} & L/2 \le R \end{cases}$$

$$d/\alpha = \begin{cases} 0.611 & R < H/2 \\ 0.611\,(H/2R) & H/2 \le R < L/2 \\ 0.611\,(H/2R)\,(L/2R) & L/2 \le R \end{cases}$$

The fits are compared with the data in Figures 13 through 18 for the cylindrical and spherical regions. Only a few data points were available in the planar region, and general comparisons with the fit are not shown. The agreement is generally good, with reasonable scatter considering the wide range of conditions under which the data were taken. During the Yuma series a vertical, cylindrical charge was detonated, and

DIHEST VELOCITY DATA

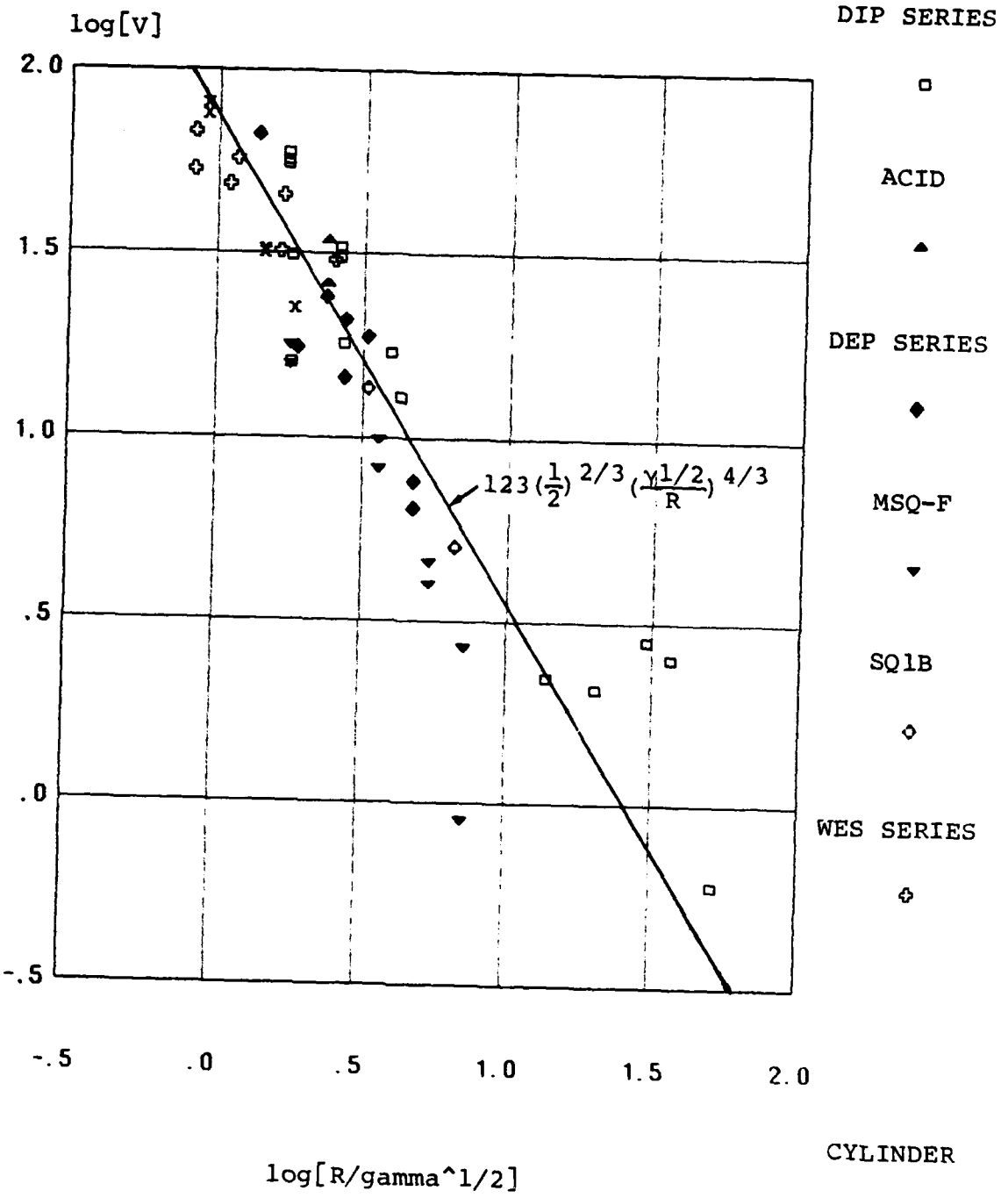

Figure 13. Cylindrical velocity attenuation.

DIHEST ACCELERATION DATA

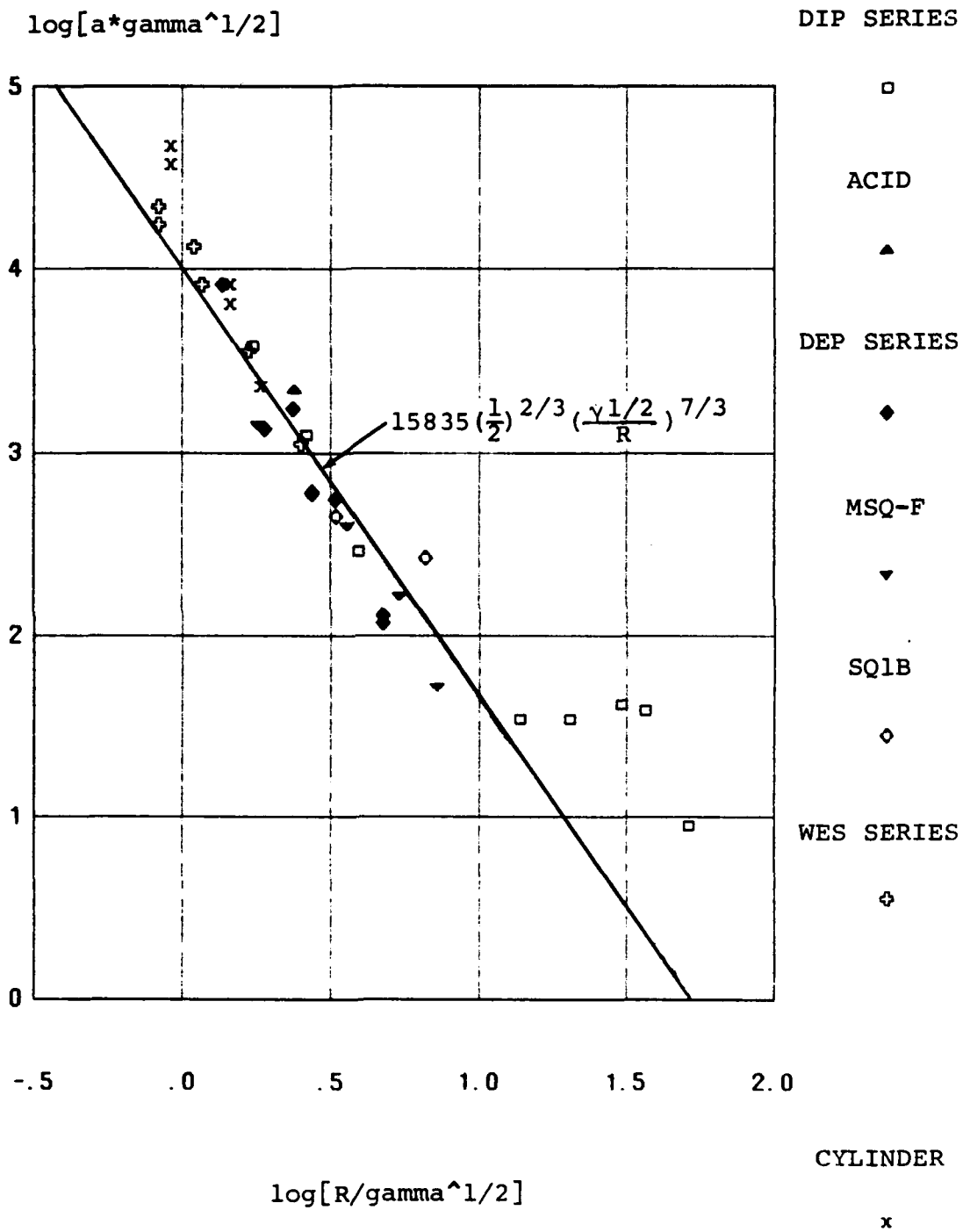

Figure 14. Cylindrical acceleration attenuation.

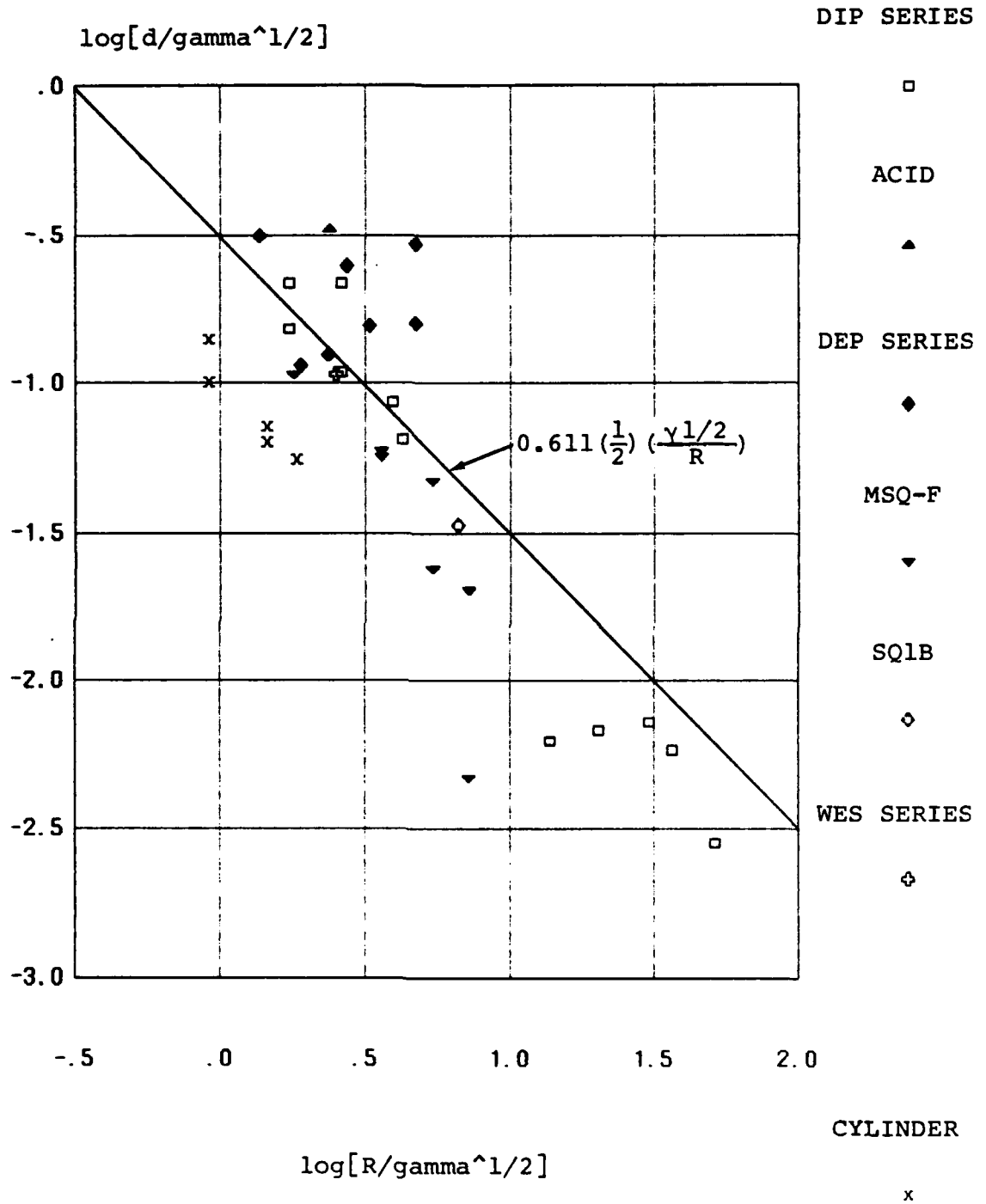

Figure 15. Cylindrical displacement attenuation.

DIHEST VELOCITY DATA

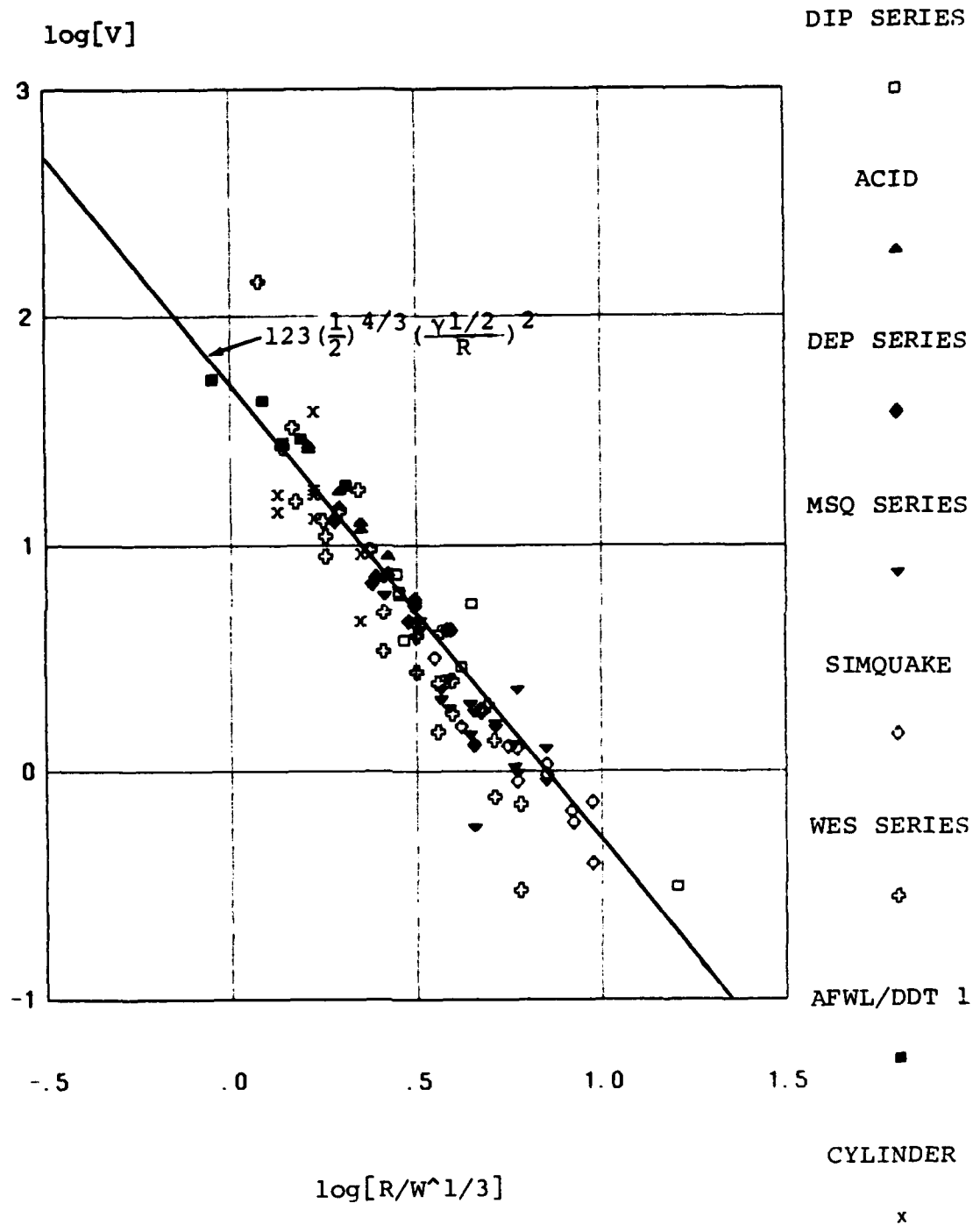

Figure 16. Spherical velocity attenuation.

DIHEST ACCELERATION DATA

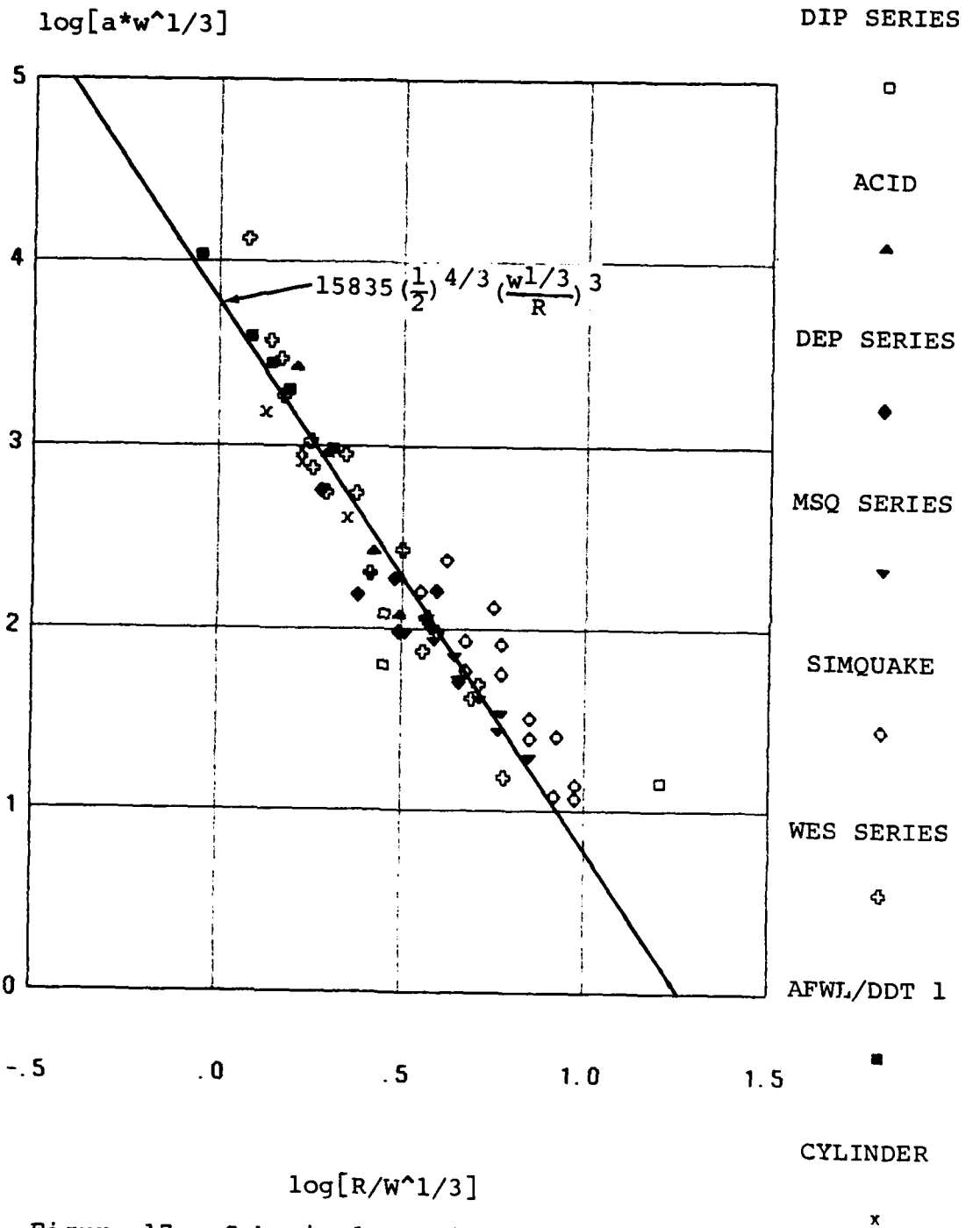

Figure 17. Spherical acceleration attenuation.

DIHEST DISPLACEMENT DATA

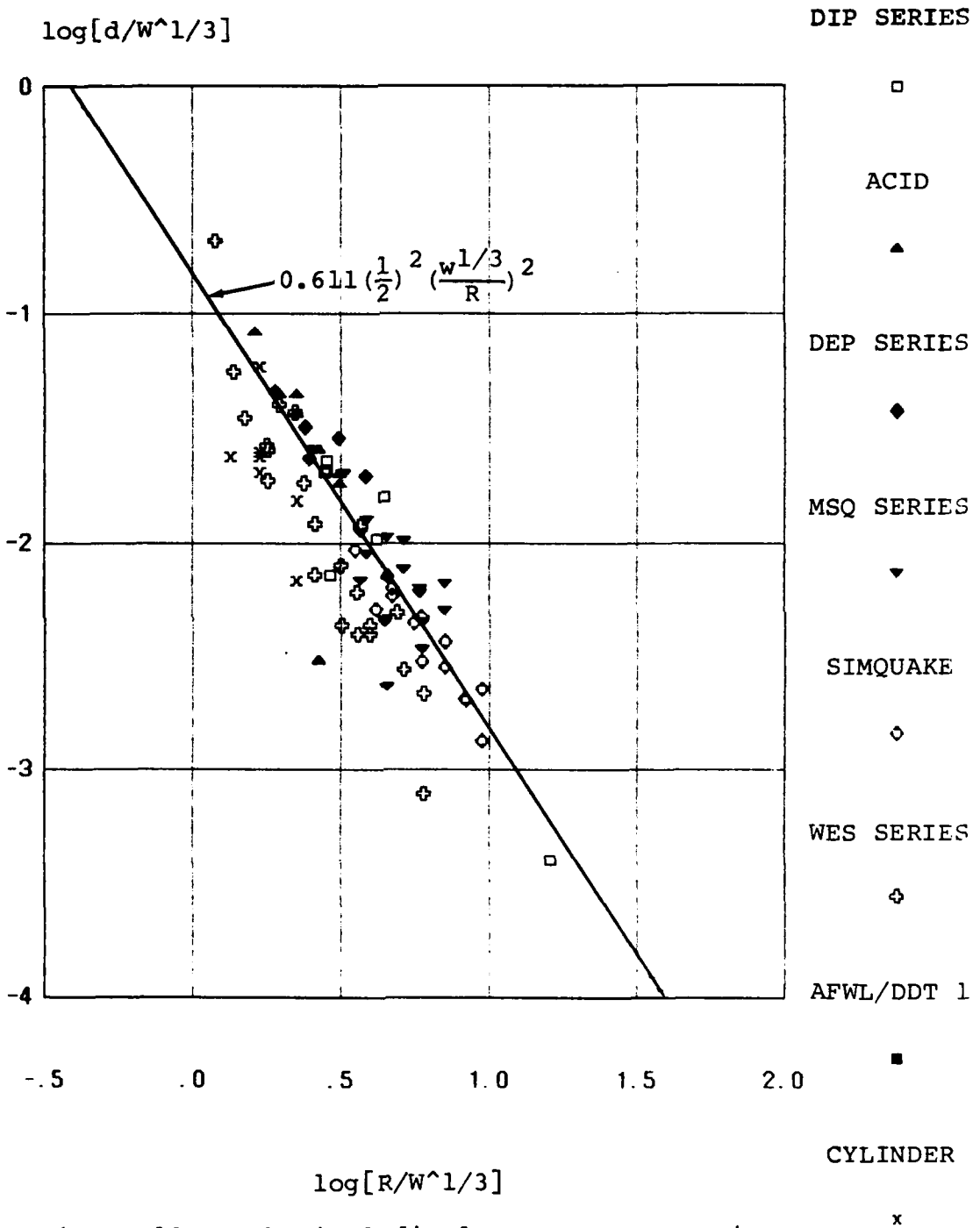

Figure 18. Spherical displacement attenuation.

those results are also shown in the figures. The cylindrical test's acceleration and velocity are described well by Drake's equations, but the displacements fall below the predictions. It is worth noting that the displacement data exhibit greater scatter than that for velocity and acceleration. This is not surprising since obtaining the peak displacement requires reliable measurement over the entire outward velocity phase, and uncertainty in reliable gauge and recording system performance is certainly greater.

The strength of Drake's approach is that for a given site, once a reliable set of data are available for a given array and in any spatial region, expressions may be directly written for predicting motions in any region. Thus, one may obtain high quality data from a single charge hole experiment, and in theory be able to derive the predictive expressions necessary to design any array for a given set of peak motions along the charge centerline in a location for which prior data do not exist.

SECTION 4
CONCLUSIONS

The available DIHEST data have been thoroughly reviewed, and greater understanding acquired about planar DIHEST array performance. Two effective predictive formulations have been developed which provide adequate accuracy for most design applications. The use of an effective length is a relatively simple fit which describes the data adequately for many purposes. Drake's approach is particularly appealing since it was structured for physical reasonableness. These demands enable one to predict peak motions at any distance along the centerline of a planar array from fits to data taken on a fairly simple calibration test.

While efforts to understand planar DIHEST arrays were fruitful, the likely direct induced simulator designs for the ISST program will involve arrays whose performance will be modified by extremely strong loads from a surface airblast simulator. The effects of pre-compaction of the soil and its effective yield strength under compressive loading must be understood, and predictive approaches developed before reliable design methods provided. Understanding DIHEST performance in combination with surface airblast simulators is a major element of the FY85 DNA simulation development program.

SECTION 5

LIST OF REFERENCES

1. Higgins, C.J., R.L. Johnson, and G.E. Triandofilidis, The Simulation of Earthquake-Like Ground Motions with High Explosives, Report No. CE-45(78)NSF-507-1 on NSF Grant ENG 75-21580, The University of New Mexico, Albuquerque, New Mexico, July 1978.

2. Higgins, C.J., et.al., SIMQUAKE I - An Explosive Test Series Designed to Simulate the Effects of Earthquake-Like Ground Motions on Nuclear Power Plant Models, Report No. NP-1728, on EPRI Project 810, The University of New Mexico, Albuquerque, New Mexico, February 1981.

3. Higgins, C.J., et.al., SIMQUAKE II: A Multiple-Detonation Explosive Test to Simulate the Effects of Earthquake-Like Ground Motions on Nuclear Power Plant Models, Report No. NP-2916, on EPRI Projects 810-1, 810-6, The University of New Mexico, Albuquerque, New Mexico, October 1983.

4. Advanced Silo Hardness Program DIHEST Development Test Plan, DNA Contract No. DNA001-84-C-0069, Applied Research Associates, Albuquerque, New Mexico, Feb. 1984.

5. Drake, J.L., Consistent Scaling of DIHEST Ground Motions, Applied Research Associates, Inc., Southern Division, Vicksburg, MS, Presented to Advanced Silo Hardness Simulation Working Group, 28-29 August 1984.

6. Private communication with Jim Drake.

APPENDIX A

BASIC DIHEST PARAMETERS AND KINEMATIC DATA

This appendix presents the data used to generate the predictive relationships for the peak values of kinematic variables associated with horizontal motions along the centerline of a DIHEST array. The data were grouped into five test series groups, according to the chronological sequence in which they were executed. The first group of data are from the DIHEST Enhancement Program (DEP) performed at the Civil Engineering Research Center for the Air Force Weapons Laboratory at the McCormick Ranch test site south of Albuquerque, New Mexico. The second series was called the DIHEST Improvement Program (DIP) which was also performed at McCormick Ranch. A later test named ACID was also fired at McCormick Ranch for AFWL, and is included with the DIP data. The third test series group was performed by the New Mexico Engineering Research Institute (NMERI) as part of an earthquake simulation program at the McCormick Ranch test site, and was designated SIMQUAKE. A series of tests is underway at the Yuma test site under the auspices of the joint DNA/BMO small missile program. This series is being conducted by the U.S. Army Waterways Experiment Station (WES), and the series is designated here as the WES series. The final series whose data are included are the DIHEST development tests (DDT) being conducted by NMERI for AFWL at the McCormick Ranch under the joint DNA/BMO small missile program.

DEP DATA

Shot	l(ft)	h(ft)	b(ft)	d(in)	s(ft)	alpha(#/sf)	R(ft)	a(g)	V(fps)	d(ft)
DEP 1	12	4	4			1.25	2	4000	52	
							4	102	4.4	.075
							12	44	6.5	.2
DEP 3	20	6.7	6	4	1.33	1.25	5.5	460	17.5	.33
							9.5	191	18.7	.45
							13.5	27	6.7	.18
							17.5	17	5.4	.16
							21.5	18	4.2	.11
							25.5	9	1.3	.04
DEP 9	40	13.3	8			4.88	11	1031	67	2.52
							19	214	24.2	1
							27	40	12.8	.64
							35		7.2	.333
DEP 13	40	13.3	8	9.4	4	1.22	11	150	14.5	
							11	147	20.8	1
							19	32	7.6	1.18
							19	29	6.4	.64
							27	21	4.6	1.64
							35	18	4.2	2.68

DIP DATA

Shot	l(ft)	h(ft)	b(ft)	d(in)	s(ft)	alpha(#/sf)	R(ft)	a(g)	V(fps)	d(ft)
DIP IIA	208	35	30	12	7.127	15.16	40	165	56	5
							40		57	3.5
							40		60	3.5
							60	54	33	5
							60		31	2.5
							90	12.5	17	2
							135	2.5	6.2	1.1
							135	1.3	6	1
							200		2.9	.5
DIP IIIA	107.5	33	20	5 decoupled hole	7.167	2.57	16.5		31.5	
							16.5		16	
							25		18	
							39		12.8	.6
							58		7.4	.42
							61		3.8	.15
							92		5.5	.33
DIP VA	1136	204	60	6.3	71	.48	60	13	4.1	.058
							90	16	4.8	.1
							135	3.5	2.2	.062
							200	3.5	2.05	.067
							300	4.2	2.8	.071
							360	3.9	2.5	.057
							510	.9	.6	.028
							770	.3	.31	.019
ACID	90	30	10	15	6.92	9.45	40		26.2	
							40	130	34.4	5.57
							48		26.9	
							48	90	26.2	2.45
							57.7		14.8	1.31
							57.7	30	17.1	
							65.9		11.5	1.08
							65.9		12.4	1.31
							78		8.9	.089
							78	9	7.5	.75
							91.8		5.9	.59
							91.8	4	5.7	.53

SQ DATA

Shot	l(ft)	h(ft)	b(ft)	d(in)	s(ft)	alpha(#/sf)	R(ft)	a(g)	V(fps)	d(ft)
MSQ-F	40	15	5	6	2.5	.52	5	500	15.75	
							5		17.72	.295
							10	142	8.2	.164
							10		9.84	.157
							15	58	4.59	.131
							15		3.97	.066
							20	18.6	2.66	.056
							20		.89	.013
							25	16.2	2.07	.046
							25		2.3	.075
							30	10.3	1.44	.031
							30		1.97	.03
							40	5	.98	.023
							40		2.3	.03
MSQ-B	40	15	5	6	3.33	.77	20	25	7.05	
							20		5.91	.197
							25	12	4.2	.154
							25		4.59	.157
							30	11	2.56	.098
							30		1.9	.069
							35	6.7	1.8	.082
							35		.56	.018
							40	5.2	1.54	.079
							40		1.64	.059
							45	3.5	1.03	.048
							45		1.31	.046
							55	2.5	.89	.039
							55		1.25	.051

SQ DATA

Shot	l(ft)	h(ft)	b(ft)	d(in)	s(ft)	alpha(#/sf)	R(ft)	a(g)	V(fps)	d(ft)
SQ1A	200	75	25	18	16.67	5.02	150	3.7	3.15	.387
							200	1.37	1.8	.243
							250	1.91	.89	.125
							300	.58	.95	.118
							400	.27	.39	.056
SQ1B	200	75	25	12	12.5	3.07	50	29	13.45	
							100	17.3	5.02	.505
							150	6.5	1.57	.18
							200	3.55	1.28	.157
							300	.7	.59	.072
SQIIB	200	75	25	16	16.67	5.02	200	2	1.87	.262
							250	1.3	1.25	.197
							300	.75	1.05	.154
							350	.28	.66	.085
							400	.32	.72	.095
SQIIF	200	75	25	12	12.5	3.35	100	26	5.91	.591
							150	15.2	3.25	.361
							200	5.05	2	.213
							250	1.4	.92	.108
							300	.97	1.05	.128

WES DATA

Shot	l(ft)	h(ft)	b(ft)	d(in)	s(ft)	alpha(#/sf)	R(ft)	a(g)	V(fps)	d(ft)
WES-1	20	20	10	6	1.67	11.50	20	809.4	144.5	3.5
							25	111	15.5	.58
							30		8.9	.31
							30	45	10.9	.42
							43		3.4	.12
							43	12	5.03	.2
							60		1.5	.066
							60	4.5	2.45	.1
							100		.3	.013
							100	.92	.71	.036
WES-4	20	20	10	12	1.67	40.40	35	146.2	26.7	1.4
							45	41.37	12.7	.67
							60	21.49	9.41	.46
							80	10.66	3.96	.2
							80		2.73	.11
							100	3.76	2.5	.11
							100		1.8	.1
							130	1.96	1.37	.07
							130		.77	.04
WES-5	30	10	5	4	1	8.27	10	1470	48.9	
							15		32.1	
							20	215	32.8	
							30	66	17.2	.5
							50	8.5	4.1	.16
WES-6	90	30	15	12	6	10.63	15	1235	67.9	
							15	987	53.5	
							21	460	57.4	
							30	200	45.9	
							45	62.5	30.3	1.9
							60	18.1	13.9	1.22
							150	1.34	1.96	.15

WES DATA

Shot	l(ft)	h(ft)	b(ft)	d(in)	s(ft)	alpha(#/sf)	R(ft)	a(g)	V(fps)	d(ft)
CYLINDER	.59	24	8	8		57.45	5	6741	81.8	.55
computed							5	8445	76.4	.75
from equivalent							8	1473	32.7	.35
side of a							8	1169	31.6	.39
rectangular hole							10	410.5	22.6	.3
							12	163	16.4	.21
							12		13.75	.21
							15	89	12.83	.18
							15	103	16.4	.22
							15		37.8	.52
							15		17.1	.21
							20	44.1	9.02	.135
							20		4.56	.06

AFWL DDT DATA

Shot	l(ft)	h(ft)	b(ft)	d(in)	s(ft)	alpha(#/sf)	R(ft)	a(g)	V(fps)	d(ft)
DDT-1	19	12	6	8	1.72	8.09	11	900	53	
							15	320	43	
							17	230	28	
							19	163	29	
							25	78	18	

APPENDIX B

DIHEST EFFECTIVE ARRAY LENGTH DATA CORRELATION

This appendix presents the data correlation which provided relationships which use effective array length to predict horizontal motions along the centerline of a DIHEST array. The analysis results are on spreadsheets in order of test series, as in Appendix A. The effective length, LN, as defined in equation 4, was postulated to account for array size and shape influence on the decay of peak values of velocity, acceleration and displacement with range. This approach was chosen to do a better job of collapsing the existing data than was achieved just by using the areal charge density, α, as a range normalizing factor. It should be noted that the areal charge density can be thought of as representing the effective array thickness for a given energy density explosive, and is suitable as a length scale factor if all areal charge values can be expressed in terms of some equivalent explosive; in this case, TNT.

The approach chosen to describe the influence of the effective length on the kinematic variables was essentially an extension of Higgins' process to account for the effects of the array dimensions. Higgins' fits (equations 1 through 3) had near integer exponents on the range dependency terms. Examination showed that assuming integer exponents did not significantly degrade the correlation, so the following forms were used:

$$a^* \alpha = A^*(LN/\alpha)^{pa}(R/\alpha)^{-3} \qquad \text{(B-1)}$$

$$V = V^*(LN/\alpha)^{pv}(R/\alpha)^{-2} \qquad \text{(B-2)}$$

$$d/\alpha = D^*(LN/\alpha)^{pd}(R/\alpha)^{-2} \qquad \text{(B-3)}$$

where A, V, D, pa, pv and pd were constants to be determined. While Higgins differentiated his fits between regions close to and far from the array, the data in Appendix A are almost exclusively in the far region. Thus, the fits presented here apply to ranges beyond the planar attenuation region.

To determine the coefficients in equations B-1 through B-3, the average value of the kinematic variables reduced by the spatial attenuation term $(R/\alpha)^{-n}$ were derived from the data for each test. Linear logarithmic least squares fits were obtained for reduced kinematic variables as a function of the term (LN/α) to obtain the coefficients. The three spreadsheets at the end of this appendix contain the fits. For reasons discussed in the body of this report, the data from certain of the prior tests were not used. Further, since the difference in the response of soil at the Yuma site and that of McCormick Ranch to DIHEST loads has not been evaluated, these fits exclude the Yuma data. The expressions obtained were:

$$a^*\alpha = 3021*(LN/\alpha)^{1.76}(R/\alpha)^{-3} \qquad \text{(B-4)}$$

$$V = 53*(LN/\alpha)^{1.38}(R/\alpha)^{-2} \qquad \text{(B-5)}$$

$$d/\alpha = 0.45*(LN/\alpha)^{1.76}(R/\alpha)^{-2} \qquad \text{(B-6)}$$

DEP DATA

Shot	l(ft)	h(ft)	alpha	LN	a*alpha	V	d/alpha	R/alpha	LN/alpha
Shot 1	12	4	1.25	6.00	5000.000	52.000		1.600	4.80
					127.500	4.400	.060	3.200	
					55.000	6.500	.160	9.600	
Shot 3	20	6.7	1.25	10.04	575.000	17.500	.264	4.400	8.03
					238.750	18.700	.360	7.600	
					33.750	6.700	.144	10.800	
					21.250	5.400	.128	14.000	
					22.500	4.200	.088	17.200	
					11.250	1.300	.032	20.400	
Shot 9	40	13.3	4.88	19.96	5031.280	67.000	.516	2.254	4.09
					1044.320	24.200	.205	3.893	
					195.200	12.800	.131	5.533	
						7.200	.068	7.171	
Shot 13	40	13.3	1.22	19.96	183.000	14.500		9.016	16.36
					179.340	20.800	.820	9.016	
					39.040	7.600	.967	15.574	
					35.380	6.400	.525	15.574	
					25.620	4.600	1.344	22.131	
					21.960	4.200	2.197	28.689	

DEP DATA

Shot	(R/al)^-2	V/(R/al)^-2	d/a/(r/al)^-2	(R/al)^-3	a*al/(R/al)^-3
Shot 1	3.906E-1	1.331E+2*	*	2.441E-1	2.048E+4
	9.766E-2	4.506E+1*	.61*	3.052E-2	4.178E+3
	1.085E-2	5.990E+2	14.75	1.130E-3	4.866E+4
		5.990E+2av	14.75av		2.444E+4av
Shot 3	5.165E-2	3.388E+2*	5.11*	1.174E-2	4.898E+4
	1.731E-2	1.080E+3	20.79	2.278E-3	1.048E+5
	8.573E-3	7.815E+2	16.80	7.938E-4	4.252E+4
	5.102E-3	1.058E+3	25.09	3.644E-4	5.831E+4
	3.380E-3	1.243E+3	26.03	1.965E-4	1.145E+5
	2.403E-3	5.410E+2*	13.32*	1.178E-4	9.551E+4
		1.041E+3av	20.41av		7.744E+4av
Shot 9	1.968E-1	3.404E+2	2.62	8.731E-2	5.762E+4
	6.597E-2	3.668E+2	3.11	1.694E-2	6.164E+4
	3.267E-2	3.918E+2	4.01	5.904E-3	3.306E+4
	1.945E-2	3.702E+2	3.51	2.712E-3	
		3.673E+2av	3.31av		5.077E+4av
Shot 13	1.230E-2	1.179E+3			
	1.230E-2	1.691E+3	66.64*	1.364E-3	1.315E+5
	4.123E-3	1.843E+3	234.59	2.647E-4	1.475E+5
	4.123E-3	1.552E+3	127.24	2.647E-4	1.336E+5
	2.042E-3	2.253E+3	658.40	9.225E-5	2.777E+5
	1.215E-3	3.457E+3	1807.97*	4.235E-5	5.185E+5
		1.996E+3av	340.08av		2.418E+5av

DIP DATA

Shot	l(ft)	h(ft)	alpha	LN	a*alpha	V	d/alpha	R/alpha	LN/alpha
DIP IIA	208	35	15.16	59.92	2502.198	56.000	.330	2.638	3.95
						57.000	.231	2.638	
						60.000	.231	2.638	
					818.901	33.000	.330	3.957	
						31.000	.165	3.957	
					189.560	17.000	.132	5.935	
					37.912	6.200	.073	8.902	
					19.714	6.000	.066	8.902	
						2.900	.033	13.188	
DIP IIIA	107.5	32	2.57	50.50		31.500		6.420	19.65
						16.000		6.420	
						18.000		9.728	
						12.800	.233	15.175	
						7.400	.163	22.568	
						3.800	.058	23.735	
						5.500	.128	35.798	
DIP VA	1136	204	.48	345.89	6.240	4.100	.121	125.000	720.60
					7.680	4.800	.208	187.500	
					1.680	2.200	.129	281.250	
					1.680	2.050	.140	416.667	
					2.016	2.800	.148	625.000	
					1.872	2.500	.119	750.000	
					.432	.600	.058	1062.500	
					.144	.310	.040	1604.167	
ACID	90	30	9.45	45.00		26.200		4.233	4.76
					1228.500	34.400	.589	4.233	
						26.000		5.079	
					850.500	26.200	.259	5.079	
						14.800	.139	6.106	
					283.500	17.100		6.106	
						11.500	.114	6.974	
						12.400	.139	6.974	
						8.900	.009	8.254	
					85.050	7.500	.079	8.254	
						5.900	.062	9.714	
					37.800	5.700	.056	9.714	

DIP DATA

Shot	(R/al)^-2	V/(R/al)^-2	d/a/(r/al)^-2	(R/al)^-3	a*al/(R/al)^-3
DIP IIA	1.437E-1	3.896E+2	2.29	5.449E-2	4.592E+4
	1.437E-1	3.966E+2	1.61	5.449E-2	
	1.437E-1	4.174E+2	1.61	5.449E-2	
	6.388E-2	5.166E+2	5.16	1.615E-2	5.072E+4
	6.388E-2	4.853E+2	2.58	1.615E-2	
	2.839E-2	5.988E+2	4.65	4.784E-3	3.962E+4
	1.262E-2	4.913E+2	5.75	1.417E-3	2.675E+4
	1.262E-2	4.755E+2	5.23	1.417E-3	1.391E+4
	5.749E-3	5.044E+2	5.73	4.359E-4	
		4.751E+2av	3.84av		3.538E+4av
DIP IIIA	2.426E-2	1.298E+3*		3.779E-3	*
	2.426E-2	6.595E+2*		3.779E-3	*
	1.057E-2	1.703E+3*		1.086E-3	*
	4.342E-3	2.948E+3	53.76	2.862E-4	
	1.963E-3	3.769E+3	83.23	8.700E-5	
	1.775E-3	2.141E+3	32.88	7.478E-5	
	7.804E-4	7.048E+3	164.55	2.180E-5	
		3.976E+3av	83.61av		av
DIP VA	6.400E-5	6.406E+4*	1.888E+3*	5.120E-7	1.219E+7*
	2.844E-5	1.688E+5*	7.324E+3*	1.517E-7	5.062E+7*
	1.264E-5	1.740E+5*	1.022E+4*	4.495E-8	3.738E+7*
	5.760E-6	3.559E+5*	2.423E+4*	1.382E-8	1.215E+8*
	2.560E-6	1.094E+6	5.778E+4	4.096E-9	4.922E+8
	1.778E-6	1.406E+6	6.680E+4	2.370E-9	7.898E+8
	8.858E-7	6.773E+5	6.585E+4	8.337E-10	5.182E+8
	3.886E-7	7.977E+5	1.019E+5	2.422E-10	5.944E+8
		9.938E+5av	7.307E+4av		5.986E+8av
ACID	5.581E-2	4.694E+2		1.319E-2	
	5.581E-2	6.163E+2	10.56	1.319E-2	9.317E+4
	3.876E-2	6.940E+2		7.631E-3	
	3.876E-2	6.760E+2	6.69	7.631E-3	1.115E+5
	2.682E-2	5.518E+2	5.17	4.393E-3	
	2.682E-2	6.375E+2		4.393E-3	6.453E+4
	2.056E-2	5.592E+2	5.56	2.949E-3	
	2.056E-2	6.030E+2	6.74	2.949E-3	
	1.468E-2	6.063E+2	.64*	1.778E-3	
	1.468E-2	5.110E+2	5.41	1.778E-3	4.783E+4
	1.060E-2	5.568E+2	5.89	1.091E-3	
	1.060E-2	5.379E+2	5.29	1.091E-3	3.465E+4
		5.849E+2av	6.41av		7.033E+4av

SQ DATA

Shot	l(ft)	h(ft)	alpha	LN	a*alpha	V	d/alpha	R/alpha	LN/alpha
MSQ-F	40	15	.52	21.82	259.067	15.750		9.650	41.96
						17.720	.569	9.650	
					73.575	8.200	.317	19.300	
						9.840	.303	19.300	
					30.052	4.590	.253	28.950	
						3.970	.127	28.950	
					9.637	2.660	.108	38.600	
						.890	.025	38.600	
					8.394	2.070	.089	48.250	
						2.300	.145	48.250	
					5.337	1.440	.060	57.900	
						1.970	.058	57.900	
					2.591	.980	.044	77.200	
						2.300	.058	77.200	
MSQ-B	40	15	.77	21.82		5.910	.254	25.808	28.34
					9.300	4.200	.199	32.259	
						4.590	.203	32.259	
					8.525	2.560	.126	38.711	
						1.900	.089	38.711	
					5.192	1.800	.106	45.163	
						.560	.023	45.163	
					4.030	1.540	.102	51.615	
						1.640	.076	51.615	
					2.712	1.030	.062	58.067	
						1.310	.059	58.067	
					1.937	.890	.050	70.971	
						1.250	.066	70.971	

SQ DATA

Shot	(R/al)^-2	V/(R/al)^-2	d/a/(r/al)^-2	(R/al)^-3	a*al/(R/al)^-3
MSQ-F	1.074E-2	1.467E+3*		1.113E-3	2.328E+5*
	1.074E-2	1.650E+3*	53.02*	1.113E-3	*
	2.685E-3	3.054E+3	117.90	1.391E-4	5.289E+5
	2.685E-3	3.665E+3	112.87	1.391E-4	
	1.193E-3	3.847E+3	211.90	4.121E-5	7.292E+5
	1.193E-3	3.327E+3	106.76	4.121E-5	
	6.712E-4	3.963E+3	161.04	1.739E-5	5.543E+5
	6.712E-4	1.326E+3*	37.38*	1.739E-5	*
	4.295E-4	4.819E+3	206.69	8.902E-6	9.429E+5
	4.295E-4	5.355E+3	336.99	8.902E-6	
	2.983E-4	4.827E+3	200.58	5.152E-6	1.036E+6
	2.983E-4	6.604E+3	194.11	5.152E-6	
	1.678E-4	5.841E+3	264.56	2.173E-6	1.192E+6
	1.678E-4	1.371E+4*	345.08	2.173E-6	*
		4.530E+3av	205.31av		7.451E+5av
MSQ-B	1.501E-3	3.936E+3	169.31	5.818E-5	
	9.609E-4	4.371E+3	206.80	2.979E-5	3.122E+5
	9.609E-4	4.777E+3	210.83	2.979E-5	
	6.673E-4	3.836E+3	189.50	1.724E-5	4.945E+5
	6.673E-4	2.847E+3	133.43	1.724E-5	
	4.903E-4	3.671E+3	215.82	1.086E-5	4.783E+5
	4.903E-4	1.142E+3*	47.38*	1.086E-5	*
	3.754E-4	4.103E+3	271.58	7.272E-6	5.541E+5
	3.754E-4	4.369E+3	202.83	7.272E-6	
	2.966E-4	3.473E+3	208.84	5.108E-6	5.311E+5
	2.966E-4	4.417E+3	200.14	5.108E-6	
	1.985E-4	4.483E+3	253.48	2.797E-6	6.926E+5
	1.985E-4	6.296E+3*	331.47*	2.797E-6	*
		4.026E+3av	205.69av		5.105E+5av

SQ DATA

Shot	l(ft)	h(ft)	alpha	LN	a*alpha	V	d/alpha	R/alpha	LN/alpha
SQ1A	200	75	5.02	109.09	18.589	3.150	.077	29.857	21.73
					6.883	1.800	.048	39.809	
					9.596	.890	.025	49.761	
					2.914	.950	.023	59.713	
					1.356	.390	.011	79.618	
SQ1B	200	75	3.07	109.09	89.088	13.450		16.276	35.53
					53.146	5.020	.164	32.552	
					19.968	1.570	.059	48.828	
					10.906	1.280	.051	65.104	
					2.150	.590	.023	97.656	
SQIIB	200	75	5.02	109.09	10.048	1.870	.052	39.809	21.73
					6.531	1.250	.039	49.761	
					3.768	1.050	.031	59.713	
					1.407	.660	.017	69.666	
					1.608	.720	.019	79.618	
SQIIF	200	75	3.35	109.09	87.100	5.910	.176	29.851	32.56
					50.920	3.250	.108	44.776	
					16.918	2.000	.064	59.701	
					4.690	.920	.032	74.627	
					3.249	1.050	.038	89.552	

SQ DATA

Shot	(R/al)^-2	V/(R/al)^-2	d/a/(r/al)^-2	(R/al)^-3	a*al/(R/al)^-3
SQ1A	1.122E-3	2.808E+3	68.67	3.757E-5	4.947E+5
	6.310E-4	2.853E+3	76.65	1.585E-5	4.342E+5
	4.038E-4	2.204E+3	61.61	8.116E-6	1.182E+6
	2.805E-4	3.387E+3	83.75	4.697E-6	6.204E+5
	1.578E-4	2.472E+3	70.66	1.981E-6	6.846E+5
		2.745E+3av	72.27av		6.833E+5av
SQ1B	3.775E-3	3.563E+3	0.0	2.319E-4	3.841E+5
	9.437E-4	5.319E+3	174.19	2.899E-5	1.833E+6
	4.194E-4	3.743E+3	139.70	8.590E-6	2.325E+6
	2.359E-4	5.425E+3	216.62	3.624E-6	3.009E+6
	1.049E-4	5.627E+3	223.52	1.074E-6	2.003E+6
		4.736E+3av	150.81av		1.911E+6av
SQIIB	6.310E-4	2.963E+3	82.64	1.585E-5	6.339E+5
	4.038E-4	3.095E+3	97.10	8.116E-6	8.048E+5
	2.805E-4	3.744E+3	109.30	4.697E-6	8.023E+5
	2.060E-4	3.203E+3	82.11	2.958E-6	4.756E+5
	1.578E-4	4.564E+3	119.87	1.981E-6	8.114E+5
		3.514E+3av	98.20av		7.056E+5av
SQIIF	1.122E-3	5.266E+3	157.20	3.760E-5	2.317E+6
	4.988E-4	6.516E+3	216.05	1.114E-5	4.571E+6
	2.806E-4	7.129E+3	226.62	4.699E-6	3.600E+6
	1.796E-4	5.124E+3	179.54	2.406E-6	1.949E+6
	1.247E-4	8.421E+3	306.42	1.392E-6	2.334E+6
		6.491E+3av	217.17av		2.954E+6av

WES DATA

Shot	l(ft)	h(ft)	alpha	LN	a*alpha	V	d/alpha	R/alpha	LN/alpha
WES-1	20	20	11.5	20.00	9308.100	144.500	.304	1.739	1.74
					1276.500	15.500	.050	2.174	
						8.900	.027	2.609	
					517.500	10.900	.037	2.609	
						3.400	.010	3.739	
					138.000	5.030	.017	3.739	
						1.500	.006	5.217	
					51.750	2.450	.009	5.217	
						.300	.001	8.696	
					10.580	.710	.003	8.696	
WES-4	20	20	40.4	20.00	5906.480	26.700	.035	.866	.50
					1671.348	12.700	.017	1.114	
					868.196	9.410	.011	1.485	
					430.664	3.960	.005	1.980	
						2.730	.003	1.980	
					151.904	2.500	.003	2.475	
						1.800	.002	2.475	
					79.184	1.370	.002	3.218	
						.770	.001	3.218	
WES-5	30	10	8.27	15.00	12156.900	48.900		1.209	1.81
						32.100		1.814	
					1778.050	32.800		2.418	
					545.820	17.200	.060	3.628	
					70.295	4.100	.019	6.046	
WES-6	90	30	10.63	45.00	13128.050	67.900		1.411	4.23
					10491.810	53.500		1.411	
					4889.800	57.400		1.976	
					2126.000	45.900		2.822	
					664.375	30.300	.179	4.233	
					192.403	13.900	.115	5.644	
					14.244	1.960	.014	14.111	

WES

Shot	(R/al)^-2	V/(R/al)^-2	d/a/(r/al)^-2	(R/al)^-3	a*al/(R/al)^-3
WES-1	3.306E-1	4.371E+2*	.92*	1.901E-1	4.896E+4*
	2.116E-1	7.325E+1	.24	9.734E-2	1.311E+4
	1.469E-1	6.057E+1	.18	5.633E-2	
	1.469E-1	7.418E+1	.25	5.633E-2	9.187E+3
	7.153E-2	4.754E+1	.15	1.913E-2	
	7.153E-2	7.032E+1	.24	1.913E-2	7.214E+3
	3.674E-2	4.083E+1	.16	7.041E-3	
	3.674E-2	6.669E+1	.24	7.041E-3	7.350E+3
	1.323E-2	2.268E+1	.09	1.521E-3	
	1.323E-2	5.369E+1	.24	1.521E-3	6.957E+3
		5.664E+1av	1.972E-1av		1.546E+4av
WES-4	1.332E+0	2.004E+1	.03	1.538E+0	3.841E+3
	8.060E-1	1.576E+1	.02	7.236E-1	2.310E+3
	4.534E-1	2.076E+1	.03	3.053E-1	2.844E+3
	2.550E-1	1.553E+1	.02	1.288E-1	3.344E+3
	2.550E-1	1.070E+1	.01	1.288E-1	
	1.632E-1	1.532E+1	.02	6.594E-2	2.304E+3
	1.632E-1	1.103E+1	.02	6.594E-2	
	9.658E-2	1.419E+1	.02	3.001E-2	2.638E+3
	9.658E-2	7.973E+0	.01	3.001E-2	
		1.459E+1av	1.798E-2av		2.880E+3av
WES-5	6.839E-1	7.150E+1		5.656E-1	2.149E+4
	3.040E-1	1.056E+2		1.676E-1	
	1.710E-1	1.918E+2		7.070E-2	2.515E+4
	7.599E-2	2.263E+2	.80	2.095E-2	2.606E+4
	2.736E-2	1.499E+2	.71	4.525E-3	1.554E+4
		1.490E+2av	7.514E-1av		2.206E+4av
WES-6	5.022E-1	1.352E+2		3.559E-1	3.689E+4
	5.022E-1	1.065E+2		3.559E-1	2.948E+4
	2.562E-1	2.240E+2		1.297E-1	3.770E+4
	1.256E-1	3.656E+2		4.449E-2	4.779E+4
	5.580E-2	5.430E+2	3.20	1.318E-2	5.040E+4
	3.139E-2	4.428E+2	3.66	5.561E-3	3.460E+4
	5.022E-3	3.903E+2	2.81	3.559E-4	4.002E+4
		3.154E+2av	3.223E+0av		3.955E+4av

WES DATA

Shot	l(ft)	h(ft)	alpha	LN	a*alpha	V	d/alpha	R/alpha	LN/alpha
CYLINDER	.59	24	57.45	1.15387	270.450	81.800	.010	.087	.02
	computed				485165.250	76.400	.013	.087	
	from equivalent				84623.850	32.700	.006	.139	
	side of a				67159.050	31.600	.007	.139	
	rectangular hole				23583.225	22.600	.005	.174	
					9364.350	16.400	.004	.209	
						13.750	.004	.209	
					5113.050	12.830	.003	.261	
					5917.350	16.400	.004	.261	
						37.800	.009	.261	
						17.100	.004	.261	
					2533.545	9.020	.002	.348	
						4.560	.001	.348	

WES DATA

Shot	(R/al)^-2	V/(R/al)^-2	d/a/(r/al)^-2	(R/al)^-3	a*al/(R/al)^-3
CYLINDER	1.320E+2	6.196E-1	7.252E-5	1.517E+3	2.553E+2
	1.320E+2	5.787E-1	9.889E-5	1.517E+3	3.198E+2
	5.157E+1	6.341E-1	1.181E-4	3.703E+2	2.285E+2
	5.157E+1	6.128E-1	1.316E-4	3.703E+2	1.813E+2
	3.301E+1	6.847E-1	1.582E-4	1.896E+2	1.244E+2
	2.292E+1	7.155E-1	1.595E-4	1.097E+2	8.534E+1
	2.292E+1	5.999E-1	1.595E-4	1.097E+2	
	1.467E+1	8.746E-1	2.136E-4	5.618E+1	9.101E+1
	1.467E+1	1.118E+0	2.611E-4	5.618E+1	1.053E+2
	1.467E+1	2.577E+0	6.170E-4	5.618E+1	
	1.467E+1	1.166E+0	2.492E-4	5.618E+1	
	8.251E+0	1.093E+0	2.848E-4	2.370E+1	1.069E+2
	8.251E+0	5.526E-1	1.266E-4	2.370E+1	
		9.097E-1av	2.039E-4av		1.664E+2av

AFWL DDT DATA

Shot	l(ft)	h(ft)	alpha	LN	a*alpha	V	d/alpha	R/alpha	LN/alpha
DDT-1	19	12	8.09	14.71	7285.263	53.000		1.359	1.82
					2590.316	43.000		1.853	
					1861.789	28.000		2.100	
					1319.442	29.000		2.347	
					631.389	18.000		3.088	

AFWL DDT

Shot	(R/al)^-2	V/(R/al)^-2	d/a/(r/al)^-2	(R/al)^-3	a*al/(R/al)^-3
DDT-1	5.415E-1	9.787E+1		3.985E-1	1.828E+4
	2.912E-1	1.477E+2		1.572E-1	1.648E+4
	2.267E-1	1.235E+2		1.080E-1	1.725E+4
	1.815E-1	1.598E+2		7.733E-2	1.706E+4
	1.048E-1	1.717E+2		3.395E-2	1.860E+4
		1.401E+2av			1.753E+4av

LSQRS(V)

TEST		LN/alpha	V/(∂/R)2	Xi ln{LN/∂}	Yi ln{V/(∂/R)2}	ΣXi	ΣYi	Σ(xi)^2	ΣXi*Yi	n
DEP 1		4.8	5.990E+2	1.57	6.40	1.57	6.40	2.46	10.03	1
DEP 3		8.03	1.041E+3	2.08	6.95	3.65	13.34	6.80	24.51	2
DEP 9		4.09	3.670E+2	1.41	5.91	5.06	19.25	8.78	32.82	3
DEP 13	*	16.39	1.996E+3	2.80	7.60	5.06	19.25	8.78	32.82	3
DIP IIA		3.95	4.751E+2	1.37	6.16	6.43	25.41	10.67	41.29	4
DIP IIIA	*	19.65	3.976E+3	2.98	8.29	6.43	25.41	10.67	41.29	4
DIP VA		720.6	9.938E+5	6.58	13.81	13.01	39.22	53.97	132.16	5
ACID		4.76	5.849E+2	1.56	6.37	14.57	45.59	56.40	142.10	6
MSQ-F		41.96	4.530E+3	3.74	8.42	18.31	54.01	70.37	173.56	7
MSQ-B		28.34	4.026E+3	3.34	8.30	21.66	62.31	81.55	201.31	8
SQIA		21.73	2.745E+3	3.08	7.92	24.73	70.23	91.03	225.69	9
SQIB		35.53	4.736E+3	3.57	8.46	28.30	78.69	103.78	255.91	10
SQIIF		21.73	6.491E+3	3.08	8.78	31.38	87.47	113.25	282.93	11
SQIIB		32.56	3.514E+3	3.48	8.16	34.87	95.63	125.39	311.37	12
WES-1	*	1.74	5.664E+1	.55	4.04	34.87	95.63	125.39	311.37	12
WES-4	*	.5	1.459E+1	-.69	2.68	34.87	95.63	125.39	311.37	12
WES-5	*	1.81	1.490E+2	.59	5.00	34.87	95.63	125.39	311.37	12
WES-6	*	4.23	3.154E+2	1.44	5.75	34.87	95.63	125.39	311.37	12
DDT-1		1.82	1.401E+2	.60	4.94	35.47	100.58	125.75	314.33	13

* indicates *value not* used in fit

slope = 1.38

intercept = 3.98

e^int = 53.42

LSQRS(a*al)

TEST		LN/alpha	a*∂/(∂/R)3	Xi ln{LN/∂}	Yi ln{a*∂/(∂/R)3}	∑Xi	∑Yi	∑(xi)^2	∑Xi*Yi	n
DEP 1		4.8	2.444E+4	1.57	10.10	1.57	10.10	2.46	15.85	1
DEP 3		8.03	7.744E+4	2.08	11.26	3.65	21.36	6.80	39.30	2
DEP 9		4.09	5.077E+4	1.41	10.84	5.06	32.20	8.78	54.56	3
DEP 13	*	16.39	2.418E+5	2.80	12.40	5.06	32.20	8.78	54.56	3
DIP IIA		3.95	3.538E+4	1.37	10.47	6.43	42.67	10.67	68.95	4
DIP VA		720.6	5.986E+8	6.58	20.21	13.01	62.88	53.97	201.93	5
ACID		4.76	7.033E+4	1.56	11.16	14.57	74.04	56.40	219.35	6
MSQ-F		41.96	7.451E+5	3.74	13.52	18.31	87.56	70.37	269.87	7
MSQ-B		28.34	5.105E+5	3.34	13.14	21.66	100.71	81.55	313.83	8
SQIA		21.73	6.833E+5	3.08	13.43	24.73	114.14	91.03	355.19	9
SQIB		35.53	1.911E+6	3.57	14.46	28.30	128.60	103.78	406.83	10
SQIIF		21.73	7.056E+5	3.08	13.47	31.38	142.07	113.25	448.29	11
SQIIB		32.56	2.954E+6	3.48	14.90	34.87	156.97	125.39	500.18	12
WES-1	*	1.74	1.546E+4	.55	9.65	34.87	156.97	125.39	500.18	12
WES-4	*	.5	2.880E+3	-.69	7.97	34.87	156.97	125.39	500.18	12
WES-5	*	1.81	2.206E+4	.59	10.00	34.87	156.97	125.39	500.18	12
WES-6	*	4.23	3.955E+4	1.44	10.59	34.87	156.97	125.39	500.18	12
DDT-1		1.82	1.753E+4	.60	9.77	35.47	166.74	125.75	506.03	13

* indicates value not used in fit

slope = 1.76

intercept = 8.01

e^int = 3020.89

LSQRS(d/∂)

TEST		LN/alpha	d/∂/(∂/R)2	Xi ln{LN/∂}	Yi ln{d/∂/(∂/R)2}	ΣXi	ΣYi	Σ(xi)^2	ΣXi*Yi	n
DEP 1		4.8	1.475E+1	1.57	2.69	1.57	2.69	2.46	4.22	1
DEP 3		8.03	2.041E+1	2.08	3.02	3.65	5.71	6.80	10.50	2
DEP 9		4.09	3.310E+0	1.41	1.20	5.06	6.90	8.78	12.19	3
DEP 13	*	16.39	3.401E+2	2.80	5.83	5.06	6.90	8.78	12.19	3
DIP IIA		3.95	3.840E+0	1.37	1.86	6.43	8.76	10.67	14.75	4
DIP IIIA*		19.65	8.361E+1	2.98	4.43	6.43	8.76	10.67	14.75	4
DIP VA		720.6	7.307E+4	6.58	11.20	13.01	19.96	53.97	88.44	5
ACID		4.76	6.410E+0	1.56	1.86	14.57	21.82	56.40	91.34	6
MSQ-F		41.96	2.053E+2	3.74	5.32	18.31	27.15	70.37	111.23	7
MSQ-B		28.34	2.057E+2	3.34	5.33	21.66	32.47	81.55	129.04	8
SQIA		21.73	7.227E+1	3.08	4.28	24.73	36.75	91.03	142.22	9
SQIB		35.53	1.508E+2	3.57	5.02	28.30	41.77	103.78	160.13	10
SQIIF		21.73	2.172E+2	3.08	5.38	31.38	47.15	113.25	176.70	11
SQIIB		32.56	9.820E+1	3.48	4.59	34.87	51.74	125.39	192.67	12
WES-1	*	1.74	1.972E-1	.55	-1.62	34.87	51.74	125.39	192.67	12
WES-4	*	.5	1.798E-2	-.69	-4.02	34.87	51.74	125.39	192.67	12
WES-5	*	1.81	7.514E-1	.59	-.29	34.87	51.74	125.39	192.67	12
WES-6	*	4.23	3.223E+0	1.44	1.17	34.87	51.74	125.39	192.67	12

* indicates value not used in fit

slope = 1.76

intercept = -.80

e^int = .45

DISTRIBUTION LIST

DEPARTMENT OF DEFENSE

DEFENSE INTELLIGENCE AGENCY
ATTN: RTS-2B

DEFENSE NUCLEAR AGENCY
ATTN: SPSS K GOERING
4 CYS ATTN: STTI-CA

DEFENSE TECHNICAL INFORMATION CENTER
12 CYS ATTN: DD

FIELD COMMAND DEFENSE NUCLEAR AGENCY
ATTN: FCTT W SUMMA

JOINT STRAT TGT PLANNING STAFF
ATTN: JPPFM
ATTN: JPSS
ATTN: JPTM

DEPARTMENT OF THE ARMY

BMD SYSTEMS COMMAND
ATTN: BMDSC-LEH R C WEBB

DEPARTMENT OF THE AIR FORCE

AIR FORCE WEAPONS LABORATORY, AFSC
ATTN: NTED E SEUSY
ATTN: NTED R HENNY
ATTN: NTEO
ATTN: NTES
ATTN: NTES J REINKE

BALLISTIC MISSILE OFFICE/DAA
ATTN: MGEN
ATTN: MGESS

STRATEGIC AIR COMMAND
ATTN: XPFC

STRATEGIC AIR COMMAND
ATTN: XPFS

DEPARTMENT OF ENERGY

LAWRENCE BERKELEY NATIONAL LAB
ATTN: P COLELLA

LOS ALAMOS NATIONAL LABORATORY
ATTN: S GARDNER
ATTN: T COOK

DEPARTMENT OF DEFENSE CONTRACTORS

AEROSPACE CORP
ATTN: H MIRELS
ATTN: L SELZER

APPLIED RESEARCH ASSOCIATES, INC
ATTN: J DRAKE

APPLIED RESEARCH ASSOCIATES, INC
ATTN: N HIGGINS

APPLIED RESEARCH ASSOCIATES, INC
ATTN: J SHINN

BDM CORP
ATTN: CORPORATE LIB

BOEING CO
ATTN: M/S 1F-72 R SCHMIDT
ATTN: M/S 13-13 S STRACK

CALIFORNIA RESEARCH & TECHNOLOGY, INC
ATTN: K KREYENHAGEN

H-TECH LABS, INC
ATTN: B HARTENBAUM

KAMAN SCIENCES CORP
ATTN: E CONRAD

KAMAN TEMPO
ATTN: DASIAC

KAMAN TEMPO
ATTN: DASIAC

MARTIN MARIETTA DENVER AEROSPACE
ATTN: E SPARKHAWK
ATTN: R HAYMEN

NEW MEXICO ENGINEERING RESEARCH INSTITUTE
ATTN: G LEIGH
ATTN: N BAUM

PACIFIC-SIERRA RESEARCH CORP
ATTN: H BRODE, CHAIRMAN SAGE

PACIFICA TECHNOLOGY
ATTN: R ALLEN

PHYSICS INTERNATIONAL CO
ATTN: H W WAMPLER

R & D ASSOCIATES
ATTN: A KUHL
ATTN: D SHRINIVASA
ATTN: J LEWIS
ATTN: P HAAS

R & D ASSOCIATES
2CYS ATTN: J WEBSTER

RAND CORP
ATTN: P DAVIS

RAND CORP
ATTN: B BENNETT

DEPARTMENT OF DEFENSE CONTRACTORS (CONT)

S-CUBED
ATTN: D GRINE
ATTN: K PYATT

SCIENCE & ENGRG ASSOCIATES, INC
ATTN: J STOCKTON

SCIENCE APPLICATIONS INTL CORP
ATTN: P VERSTEEGEN

SCIENCE APPLICATIONS INTL CORP
ATTN: N KFOURY

SCIENCE APPLICATIONS INTL CORP
ATTN: G BINNINGER

SRI INTERNATIONAL
ATTN: J COLTON

TECH REPS, INC
ATTN: D NORTON

TERRA TEK, INC
ATTN: S GREEN

TRW ELECTRONICS & DEFENSE SECTOR
ATTN: J BELL

TRW ELECTRONICS & DEFENSE SECTOR
ATTN: G HULCHER
ATTN: H KORMAN
ATTN: P DAI

WEIDLINGER ASSOC, CONSULTING ENGRG
ATTN: M BARON

WEIDLINGER ASSOC, CONSULTING ENGRG
ATTN: H LEVINE

END

DTIC

5-86